iScience

CellPress
OPEN ACCESS

Article

Novel requirements for HAP2/GCS1-mediated gamete fusion in *Tetrahymena*

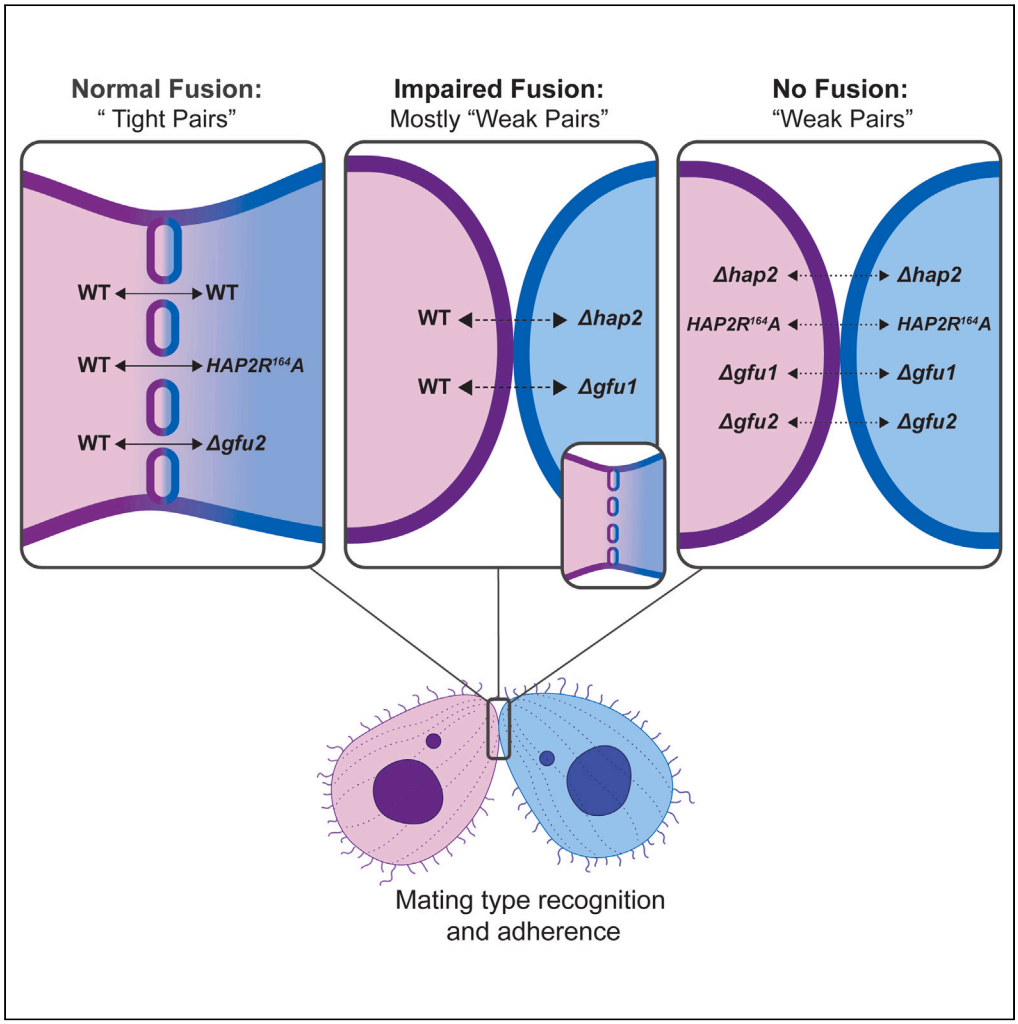

Jennifer F. Pinello, Josef Loidl, Ethan S. Seltzer, ..., Timothy Maugel, Eric S. Cole, Theodore G. Clark

tgc3@cornell.edu

Highlights

Tetrahymena mating pairs fail to form fusion pores in the absence of GFU1 or GFU2

GFU1 has a predicted BAR-like domain structure, while GFU2 is membrane-spanning

Like HAP2/GCS1, GFU1 is required in both mating cells to ensure efficient fusion

A model of cooperativity between the fusion machinery on mating cells is proposed

Pinello et al., iScience *27*, 110146
June 21, 2024
https://doi.org/10.1016/j.isci.2024.110146

iScience

CellPress
OPEN ACCESS

Article

Novel requirements for HAP2/GCS1-mediated gamete fusion in *Tetrahymena*

Jennifer F. Pinello,[1,3,11] Josef Loidl,[2,10,11] Ethan S. Seltzer,[3,11] Donna Cassidy-Hanley,[3,11] Daniel Kolbin,[3] Anhar Abdelatif,[3] Félix A. Rey,[4,5] Rocky An,[3] Nicole J. Newberger,[3] Yelena Bisharyan,[6] Hayk Papoyan,[3] Haewon Byun,[3] Hector C. Aguilar,[3] Alex L. Lai,[7] Jack H. Freed,[7] Timothy Maugel,[8] Eric S. Cole,[9] and Theodore G. Clark[3,10,12,*]

SUMMARY

The ancestral gamete fusion protein, HAP2/GCS1, plays an essential role in fertilization in a broad range of taxa. To identify factors that may regulate HAP2/GCS1 activity, we screened mutants of the ciliate *Tetrahymena thermophila* for behaviors that mimic *Δhap2/gcs1* knockout phenotypes in this species. Using this approach, we identified two new genes, *GFU1* and *GFU2*, whose products are necessary for membrane pore formation following mating type recognition and adherence. GFU2 is predicted to be a single-pass transmembrane protein, while GFU1, though lacking obvious transmembrane domains, has the potential to interact directly with membrane phospholipids in the cytoplasm. Like *Tetrahymena* HAP2/GCS1, expression of GFU1 is required in both cells of a mating pair for efficient fusion to occur. To explain these bilateral requirements, we propose a model that invokes cooperativity between the fusion machinery on apposed membranes of mating cells and accounts for successful fertilization in *Tetrahymena's* multiple mating type system.

INTRODUCTION

The conserved transmembrane protein, HAP2/GCS1, drives gamete fusion in a vast array of species.[1,2] Interestingly, HAP2/GCS1 orthologs are structurally homologous to viral class II fusion proteins[3–5] and catalyze membrane merger by mechanisms that appear similar to those used by dengue, Zika, and related viruses for host cell entry. This begins with the activation of HAP2/GCS1 protomers at the plasma membrane of one cell (typically, the male gamete) leading to insertion of hydrophobic "fusion loops" into the lipid bilayer of the partner cell (usually the female gamete).[6–10] Activation is followed by trimerization of HAP2/GCS1 ectodomains and conformational fold-back to deform membranes and bring them close enough to allow them to fuse.[7–9,11]

While dynamic rearrangements in HAP2/GCS1 structure generate the forces necessary for gamete merger, mechanistic details around the activation of pre-fusion protomers, the possible transition of hemi-fusion intermediates to full fusion pores, and the expansion of pores to form a single contiguous membrane are only just beginning to emerge. These steps regulate both cell-cell and virus-host cell fusion in other contexts[12–14] and may be critically important for the precise spatiotemporal control of fertilization.

In flowering plants and green algae, timely activation of the HAP2/GCS1 machinery appears to be regulated in part, by accessory proteins that sequester the fusogen and/or constrain its activity prior to membrane merger. In the unicellular alga, *Chlamydomonas reinhardtii*, the lineage-specific adhesion protein, MAR1, associates either directly or indirectly with HAP2/GCS1 in *minus* ("male") gametes and is required for its correct expression and localization on a single, apical membrane protrusion known as the *minus* mating structure.[15,16] Interaction of MAR1 with the broadly conserved GEX2-like protein, FUS1, on *plus* ("female") gametes releases HAP2/GCS1 from an inactive state allowing it to drive gamete fusion at the site where mating structures of *plus* and *minus* gametes adhere.[8,15]

[1]Department of Cell Biology and Molecular Genetics, University of Maryland, College Park, MD 20742, USA
[2]Department of Chromosome Biology, Max Perutz Labs, University of Vienna, Vienna, Austria
[3]Department of Microbiology and Immunology, Cornell University, Ithaca, NY 14853, USA
[4]Unité de Virologie Structurale, Institut Pasteur, 75724 Paris, France
[5]CNRS UMR 3569, 75724 Paris, France
[6]Office of Technology Development, Harvard University, Cambridge, MA 02138, USA
[7]Department of Chemistry and Chemical Biology, Cornell University, Ithaca, NY 14850, USA
[8]Department of Biology, Laboratory for Biological Ultrastructure, University of Maryland, College Park, MD 20742, USA
[9]Biology Department, St. Olaf College, Northfield, MN 55057, USA
[10]Senior author
[11]These authors contributed equally
[12]Lead contact
*Correspondence: tgc3@cornell.edu
https://doi.org/10.1016/j.isci.2024.110146

A somewhat analogous situation has been described in the model plant species, *Arabidopsis thaliana*, where HAP2/GCS1 is initially sequestered on intracellular vesicles of male gametes through associations with the plant-specific proteins DMP8/9, until sperm and egg come into close proximity.[17] Under the influence of EC1, a secreted peptide from the egg, HAP2/GCS1 translocates to the plasma membrane of sperm where it promotes gamete fusion.[18]

Along with *Chlamydomonas* and *Arabidopsis*, the free-living ciliate, *Tetrahymena thermophila* offers a powerful system for the study of membrane dynamics during fertilization.[19] Following starvation, cells undergo a program of sexual development that generates up to seven different mating types.[20,21] A given mating type can recognize and adhere to any of the other six mating types but not its own. Fertilization can be readily synchronized and begins at a specialized region of the cell cortex known as the conjugation junction where mating cells adhere. Small (~50 nm diameter) membrane protrusions then extend into the luminal space separating cells marking the sites where HAP2/GCS1-mediated fusion pores open up.[22–24] This is followed by pore expansion and reciprocal exchange of migratory haploid pronuclei across the junction, culminating in karyogamy and, eventually, separation of cells as new progeny[23,25] (Figure S1).

Unlike sexually dichotomous species where the protein is expressed primarily in male gametes,[16,26,27] HAP2/GCS1 is produced in all seven mating types of *T. thermophila* and is required in both cells of a mating pair for efficient pore formation to occur.[3,24] This bilateral requirement is reminiscent of the developmental cell-cell fusogens, AFF-1 and EFF-1, in the nematode worm, *Caenorhabditis elegans*[28]. Like HAP2/GCS1, AFF-1 and EFF-1 are structurally homologous to class II fusion proteins of viruses but are required on adjacent membranes for multinucleated syncytia to form.[29,30] As with the viral fusogens, HAP2/GCS1 acts unilaterally from a single membrane in those species where it is expressed solely in male gametes.[16,27,31] Nevertheless, the bilateral requirements described above suggest that these structurally related fusion proteins may use different mechanisms to achieve membrane merger. Indeed, models involving *trans*-interactions between fusion proteins on apposed membranes have been proposed for the nematode protein, EFF-1,[32–35] which appears to lack a hydrophobic "fusion loop"[34] that is otherwise required to bridge membranes prior to fusion.

In *Tetrahymena*, the absence of HAP2/GCS1 from one cell of a mating pair results in a steep decline in the number of pairs capable of forming fusion pores, while its absence from both cells completely abrogates pore formation.[3] When left undisturbed, mating pairs that lack pores separate prematurely and fail to exchange meiotic pronuclei.[24] Furthermore, compared to wild type cells, pairs formed by *Δhap2/gcs1* deletion strains separate readily when mechanically agitated suggesting that junctional pores help to rivet these highly motile cells together long enough to allow them to complete fertilization.[24,36]

Based on these findings, it seemed reasonable that unstable pairing following adherence of mutant mating types might offer a useful screen to identify additional gene products involved in membrane pore formation during fertilization. Using this approach, we identified two genes designated *GFU1* and *GFU2* (Gamete FUsion 1 and 2) that are necessary for HAP2/GCS1-mediated pore formation in mating *T. thermophila*. GFU2 appears to be a small transmembrane protein, while GFU1 has properties reminiscent of BAR domain-containing proteins[37,38] that can recognize, bind to, and shape membrane structures in eukaryotes. Finally, observations of *GFU1* and *HAP2/GCS1* mutant cell lines provide strong evidence of cooperative interactions between the fusion machinery on apposed cells. A model that explains cooperativity and accounts for the expression of HAP2/GCS1 in all seven mating types of *T. thermophila* is presented.

RESULTS

Identification of genes required for stable pairing of mating cells

Sexual development in *T. thermophila* is initiated by nutrient deprivation.[19] Following starvation, physical interactions between cells of different mating types lead to rapid upregulation of genes involved in cell-cell recognition and adherence, membrane fusion, meiosis, and exchange of migratory pronuclei between mating cells resulting in karyogamy.[19–21,39,40] Initial interactions between cells are transient, but within 1.5 h post-mixing (30°C) complementary mating types begin to form mechanically stable pairs that remain adherent until they naturally separate as sexual progeny roughly 12 h after their initial interaction (Figure S1).

Using a reverse genetics approach designed to identify genes involved in conjugation,[41] we found two instances (Tetrahymena Genome Database: TTHERM_000161578, TTHERM_00569470) in which the deletion of a gene that is upregulated during this process (Figures S2A and S2B) resulted in unstable pairing between complementary mating types lacking the same gene. In each case, mutant strains recognized and adhered to one another at the conjugation junction (Figures 1A–1D) but could be separated by vigorous pipetting. As demonstrated here, we found that both genes are required for cells to form fusion pores and name them *GFU1* and *GFU2*, respectively.

To better characterize pair formation by *Δgfu1* and *Δgfu2* deletion strains, we compared the kinetics of pairing and the relative strength of cell-cell adhesion in crosses between knockout (*Δgfu* X *Δgfu*), wild type (WT X WT), and WT X *Δgfu* cell lines. When left undisturbed, complementary mating types carrying the *Δgfu1* deletion reached the same degree of pairing with roughly the same kinetics as WT X WT cultures over the first 6 h of mating (Figure 1E). Similarly, mixtures of *Δgfu2* deletion strains were also able to form pairs, albeit with slower kinetics and lower peak values than WT pairs over the same time frame (Figure 1F). In both cases, however, the pairs formed between complementary *Δgfu1* X *Δgfu1* or *Δgfu2* X *Δgfu2* deletion strains exited the sexual cycle prematurely and came apart hours before WT X WT pairs (Figures 1E and 1F). Notably, *Δgfu1* and *Δgfu2* deletion strains behaved differently from each other when mated to WT cells. Pairs formed between WT and *Δgfu1* cells had an intermediate phenotype in which many, but not all pairs, came apart prematurely (Figure 1E), while WT X *Δgfu2* cultures showed essentially the same kinetics of pairing and cell separation as WT X WT crosses (Figure 1F).

To measure the relative strength of cell-cell adhesion, mating pairs were vortexed at a fixed speed and examined microscopically for pair stability at varying intervals. As expected, WT X WT pairs were highly stable, whereas most pairs formed by *Δgfu1* X *Δgfu1* (Figure 1G) or *Δgfu2* X *Δgfu2* (Figure 1H) deletion strains came apart within 10–15 s of vortexing. When mixed with WT cells, *Δgfu1* and *Δgfu2* deletion

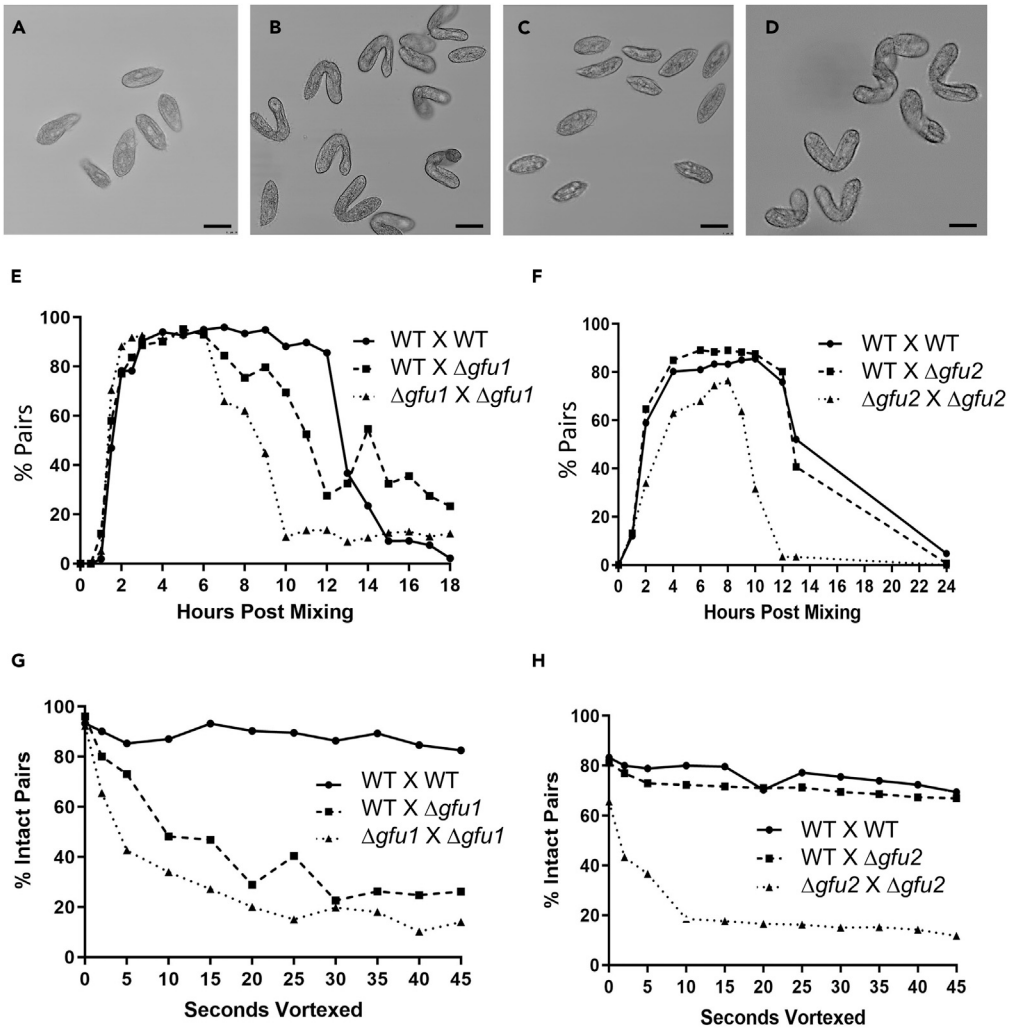

Figure 1. Characteristics of cell-cell pairing by *Δgfu1* and *Δgfu2* mutant cell lines

(A–D) Wild type and deletion strains lacking either *GFU1* or *GFU2* were starved to induce mating competency and then mixed with equal numbers of cells of complementary mating type as indicated in each panel. A–D are phase contrast images showing mixtures of *Δgfu1* (A, B) or *Δgfu2* (C, D) deletion strains fixed immediately after mixing (A, C) or 4 h post-mixing (B, D) (bar = 20 μm). Note the heart-shaped mating pairs visible at the 4 h time point in (B) and (D).

(E and F) show the kinetics of pair formation in undisturbed cultures. For (E–H), mating competent cells were mixed at ratios of 1:1, then fixed at the indicated time points and counted to determine the percentage of cells in pairs.

(G and H) show the relative stability of pairs from mating cultures of WT, *Δgfu1*, and *Δgfu2* strains following vortexing. Samples were collected from undisturbed cultures at 4 h post-mixing, vortexed at a fixed speed for the times shown on the x axis, then fixed and counted to determine the percentage of cells in pairs. (E–H) show representative data from individual experiments in each case.

strains again behaved differently from each other. Whereas WT X *Δgfu1* pairs were unstable, WT X *Δgfu2* pairs were indistinguishable from WT pairs in resisting mechanical shear (Figures 1G and 1H). Taken together, these results indicate that GFU1 (like HAP2/GCS1) is required in both cells of a mating pair for stable pairing to occur, whereas GFU2 confers pair stability when expressed in only one cell of a mating pair.

Requirements for GFU1 and GFU2 in membrane fusion

To determine whether pair instability was correlated with an inability of *Δgfu1* or *Δgfu2* deletion strains to form fusion pores, we used a previously described flow cytometry assay to measure exchange of labeled cytosolic proteins between mating cells as a proxy for membrane pore formation during fertilization.[3] In these assays, starved cells of different mating types were labeled either red or green with CellTrace Far Red (CTFR) or carboxyfluorescein succinimidyl ester (CFSE), respectively, then combined and fixed either immediately after mixing or 18–24 h post-mixing after mating pairs had separated as postzygotic progeny (Figures 2A and 2B).

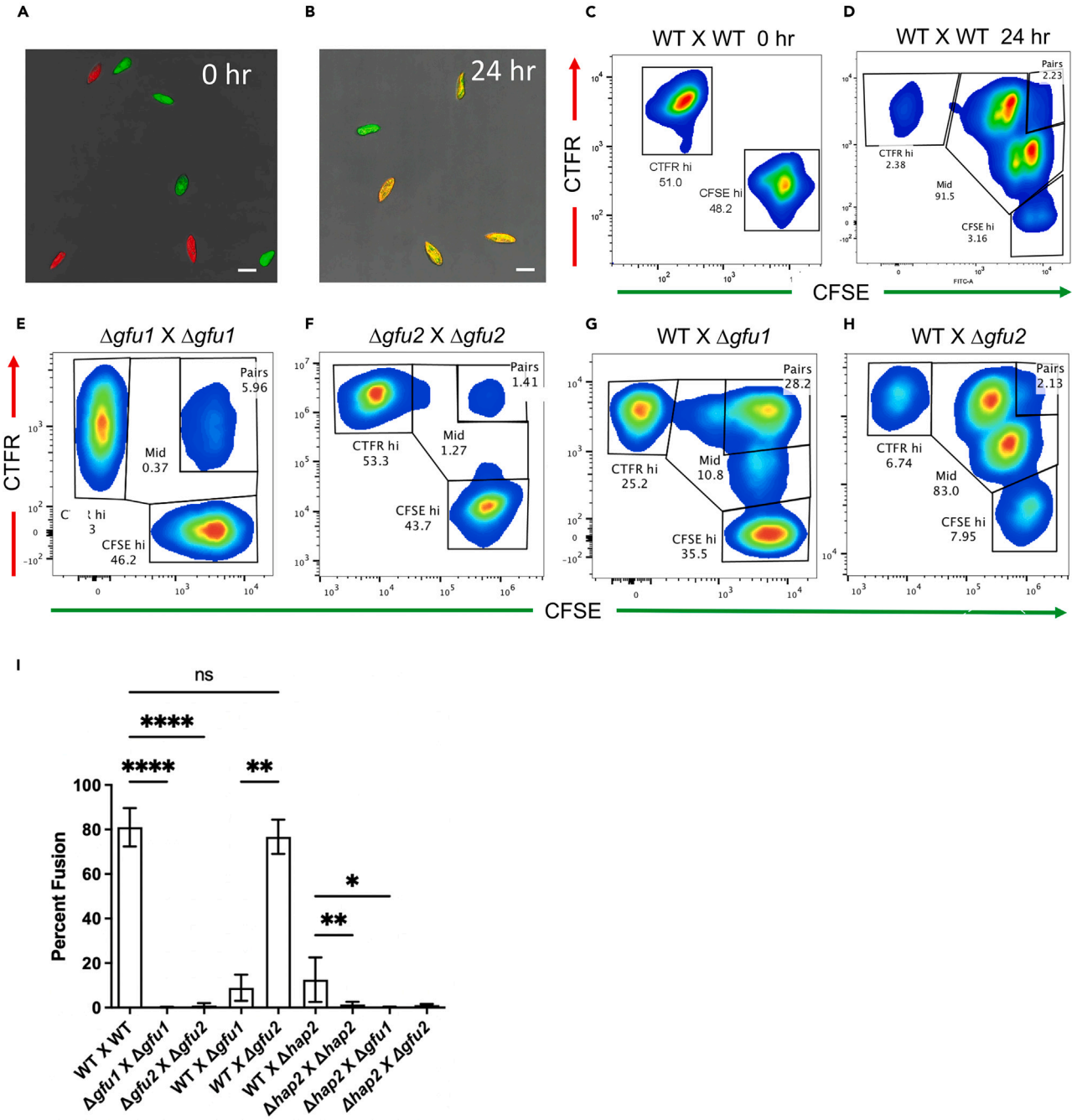

Figure 2. Quantitation of cell-cell fusion by flow cytometry

(A) and (B) are fluorescence confocal images of a mating culture of wild type *T. thermophila* containing equal numbers of cells of complementary mating type that had been labeled with CFSE (green) or CTFR (red) prior to mixing. (A) shows cells immediately after mixing (0 h), while (B) shows cells 24 h after mixing when sexual development was complete and pairs of cells had come apart. Note that cells in (A) are either red or green, while in (B), four of five cells show both colors and appear yellow (scale bar = 30 μm).

(C) and (D) are representative smoothed display pseudocolor flow cytometry plots of the same cultures imaged in (A) and (B) either before (C) or after (D) cells had undergone fusion and exchanged cytosolic proteins. Initially (0 h), only two populations were present (labeled $CTRF^{hi}$ and $CFSE^{hi}$). After fusion (24 h), the original single-labeled populations were diminished, and >90% of cells were present in two new populations labeled with both dyes (labeled "Mid" gate in (D)). An additional small population was also present at the 24 h time point labeled "Pairs". As shown previously, this gate represents cell pairs that either failed to come apart or continued to attempt to pair after normal mating was complete.[3]

(E–H) are representative flow cytometry plots of mating cultures of *Δgfu1* or *Δgfu2* deletion strains crossed to complementary mating types carrying the *Δgfu1* or *Δgfu2* deletions (panels E,F) or to WT cells (G, H) 18–24 h post-mixing.

Figure 2. *Continued*

(I) is a bar graph showing the compiled data from multiple crosses between WT, *Δgfu1*, *Δgfu2*, and *Δhap2* deletion strains as indicated on the x axis (n = 12–78 biological replicates/cross). Bars show the mean percentage of cells that had undergone fusion (calculated from the "Mid" gate) and the bracketed lines, the standard deviations (+/−). Asterisks represent the level of statistical significance between indicated crosses based on one-sided Kruskal-Wallis tests and Dunn's post-tests (**** = $p < 0.0001$; ** = $p < 0.01$; * = $p < 0.05$; ns = not significant).

Figure 2 shows representative flow cytometry plots of mating cultures containing 1:1 mixtures of WT X WT, WT X *Δgfu*, or *Δgfu* X *Δgfu* strains. When fixed immediately after mixing (0 h), two intensely labeled cell populations were always present, one bright green ($CFSE^{hi}$) and the other bright red ($CTFR^{hi}$) representing cells of each mating type before membrane fusion (Figure 2C). In WT X WT cultures, following fusion and pair separation, these initial populations were replaced almost entirely by two new populations of labeled cells, one more green than red and the other more red than green (Figure 2D). These new populations (delineated by the "Mid" gate in Figure 2D), represent single cells that had paired, formed fusion pores, and exchanged cytosolic dyes before separating as newly formed progeny. Additionally, a variable, but usually small population of $CFSE^{hi}/CTFR^{hi}$ cells was present (designated the "Pairs" gate in Figure 2D) representing cells that continue to pair even at late time points.[3]

Unlike WT X WT crosses, matings between *Δgfu1* X *Δgfu1* and *Δgfu2* X *Δgfu2* deletion strains showed little evidence of dye exchange with the percentage of cells in the "Mid" gates of the corresponding flow cytometry plots averaging <1% at 18–24 h post-mixing (Figures 2E, 2F and 2I). Thus, despite being able to form pairs, these cells, like *Δhap2/gcs1* deletion strains,[3] were unable to form stable fusion pores at the conjugation junction.

In the case of WT X *Δgfu* crosses, data from flow cytometry fusion assays were consistent with the pair stability results described above. Only a small percentage (5–15%) of cells were capable of fusion in WT X *Δgfu1* crosses (Figures 2G–2I), whereas in WT X *Δgfu2* crosses the percentage of cells capable of fusion was essentially the same as for WT X WT matings (Figures 2H and 2I). These results reinforce the idea that pore formation and pair stability are closely linked and demonstrate a bilateral versus a unilateral requirement for the *GFU1* and *GFU2* gene products, respectively, for efficient fusion between mating cells. It is also worth noting that when crossed to *Δhap2/gcs1* deletion strains, neither *Δgfu1* nor *Δgfu2* knockout cell lines showed measurable levels of fusion (Figure 2I).

Possible functional roles of GFU1 and GFU2

BLAST comparisons showed no obvious homologs outside the ciliate taxon for either GFU1 or GFU2. Furthermore, based on primary sequence analysis (Figure S2D), GFU1 bore none of the hallmarks of a transmembrane protein, despite its requirement in membrane fusion. Nevertheless, localization studies using C-terminally tagged versions of GFU1 showed bright punctate staining at the margin of the conjugation junction indicating possible interactions with membrane-associated proteins, or the membrane itself (Figures 3A–3C). GFU2, on the other hand, is almost certainly a transmembrane protein containing a predicted N-terminal signal peptide (residues 1–17), a single transmembrane helix (residues 164–186), and a cytosolic domain (residues 187–228) enriched in positively charged residues (estimated pI = 11.46) (Figure S2E).

To gain further insight into their possible function, we used AlphaFold2[46] and other structure prediction algorithms to deduce the 3-dimensional structures of both proteins. In the case of GFU2, aside from the transmembrane helix, we found only weak similarities to structures in the PDB database[47] in a region containing two sets of anti-parallel β-sheets within the putative ectodomain (Figures S3A and S3B). These similarities were not considered to be significant.

Computational modeling of GFU1, on the other hand, was more revealing. Based on AlphaFold2, the protein appeared to be almost entirely alpha-helical with its long antiparallel hairpins bearing a close structural resemblance to F-BAR (Bin/Amphiphysin/Rvs-like) domains on proteins that detect and contribute to membrane curvature[37,38] (Figure 3D). Additionally, structure prediction algorithm, RaptorX,[42] assigned high confidence homology scores linking GFU1 with 3 known F-BAR domain-containing proteins (Figure 3E).

Given its predicted structural similarity to BAR domains, we used electron spin resonance (ESR) spectroscopy to explore whether GFU1 could interact directly with lipid bilayers. We used two spin-labeled probes, DPPTC and 5PC, one labeled on its head groups (DPPTC) the other on its acyl chains (5PC) and compared the lipid ordering effects of the full-length GFU1 protein with those of known membrane interacting fusion peptides of influenza HA[48,49] and *Tetrahymena* HAP2/GCS1.[3] Spin resonance measurements with both probes showed a clear ordering effect (measured as ΔS_0) of GFU1 with increasing protein:lipid ratios (Figures 3F and 3G). At the highest ratio, the ordering effect with DPPTC was just below that seen with the HAP2/GCS1 fusion peptide (Figure 3F). By contrast, the ordering effect of GFU1 with the acyl chain labeled probe, 5PC, was considerably lower relative to the fusion peptides suggesting that its interaction with the membrane is more peripheral as might be expected for BAR domain-containing proteins, which adhere to the surfaces of membrane bilayers[37,38,50] (Figure 3G).

Additional evidence for membrane interacting effects of GFU1 came from fluorescence dequenching assays, which showed significant levels of lipid mixing following addition of GFU1 to solutions of R18-labeled and unlabeled unilamellar vesicles (Figures S4A and S4B).

GFU1 and GFU2 in heterologous cell:cell fusion assays

In previous studies, HAP2/GCS1 from *Arabidopsis thaliana* was shown to promote cell-cell fusion when expressed as a recombinant protein in mammalian tissue culture cells.[5] We therefore used this approach to explore potential interactions between GFU1, GFU2, and the HAP2/GCS1 orthologs from *Tetrahymena* and *Arabidopsis* by expressing these proteins, either alone or in combination and measuring syncytia formation in cultures of BSR-T7 baby hamster kidney cells, a standard platform for determining the fusogenic activity of viral envelope proteins.[51–53]

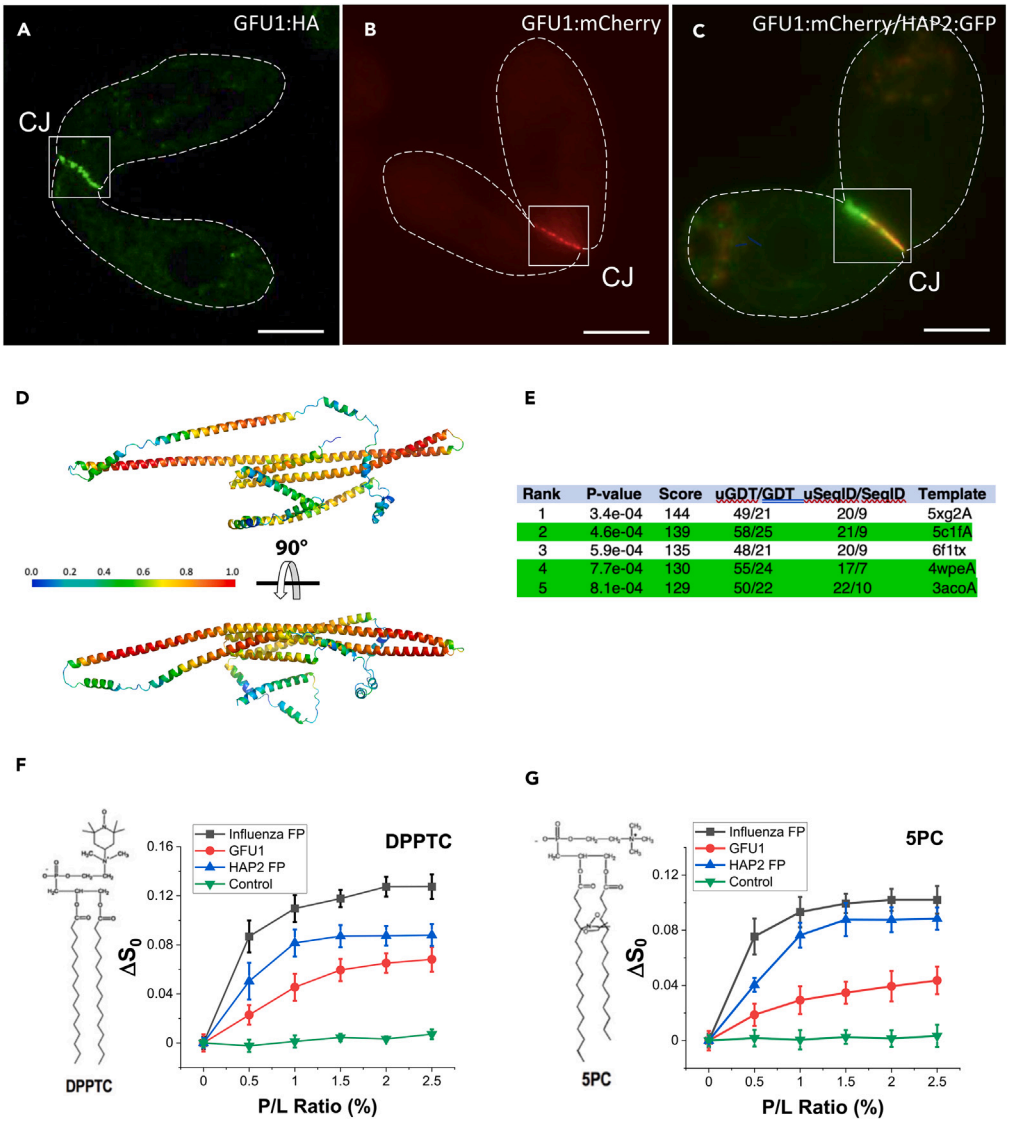

Rank	P-value	Score	uGDT/GDT	uSeqID/SeqID	Template
1	3.4e-04	144	49/21	20/9	5xg2A
2	4.6e-04	139	58/25	21/9	5c1fA
3	5.9e-04	135	48/21	20/9	6f1tx
4	7.7e-04	130	55/24	17/7	4wpeA
5	8.1e-04	129	50/22	22/10	3acoA

Figure 3. Localization and predicted structural features of GFU1

(A–C) show fluorescence light microscopic images of mating pairs formed by WT cells and transgenic cell lines expressing C-terminal HA- (A) or mCherry-tagged (B,C) versions of GFU1 from chimeric genes introduced at the endogenous *GFU1* locus. In (A), the HA-tagged gene product was detected with a fluorescein-labeled (green) secondary antibody. In (B) and (C), the mCherry-tagged construct (red) was visualized directly using confocal imaging. In (C), the labeled cell is co-expressing an inducible, GFP-tagged version of HAP2/GCS1 (green) from the β-tubulin 1 locus. White boxes indicate the conjugation junction (CJ) where mating types adhere and the dashed white lines demarcate the borders of mating cells (scale bars, lower right corner = 10 μm).

(D) shows orthogonal views of the AlphaFold2 predicted structure of GFU1. Color coding is based on prediction reliability scores with blue (0.0) representing the lowest and red (1.0) the highest confidence scores. Note the shallow curvature along the long axes of the extended α-helices in the lower image, a common feature of F-BAR domains.[37]

(E) shows the results of a structure homology search comparing GFU1 to known structures in the PDB database using RaptorX.[42] Three of the five top hits (highlighted in green) are to known F-BAR domain-containing proteins[43–45] with *p*-values and uGDT scores reflecting high quality predictions in each case.

(F) and (G) are ESR plots showing changes in the order parameter (ΔS_0) of spin-labeled lipid probes labeled on their head groups (DPPTC) or acyl chains (5PC), respectively, within multilamellar liposome vesicles as a function of increasing protein-to-lipid ratio. Plots show the relative ordering effects of recombinant GFU1 (red), compared with previously described fusion peptides from influenza virus HA (black), *Tetrahymena* HAP2/GCS1 (blue), and a corresponding scrambled peptide for the ciliate protein as a negative control (green).[3] Data points and error bars in (F) and (G) represent the means +/− standard deviations in ΔS_0 from 3 independent experiments.

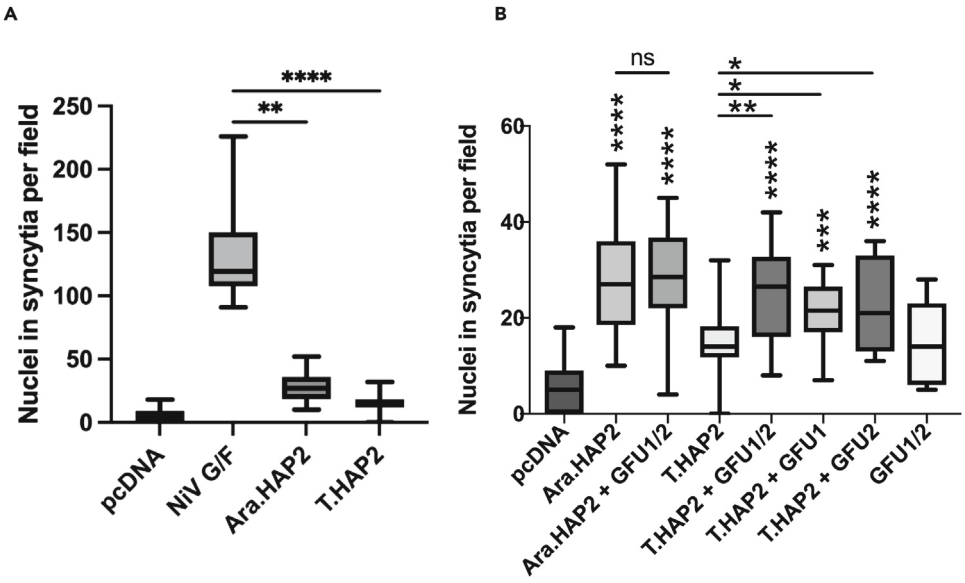

Figure 4. Heterologous cell-cell fusion assays

(A) and (B) are box and whisker plots showing levels of cell-cell fusion in BSR-T7 baby hamster kidney (BHK) cell cultures 30 h post-transfection with plasmid expression vectors encoding cDNAs indicated on the x axes. (A) shows relative levels of cell-cell fusion in cultures transfected with empty vector alone (pcDNA), or vectors encoding the Nipah virus (NiV) triggering protein G and fusion protein F (NiV G/F), or the HAP2/GCS1 orthologs of *Arabidopsis thaliana* (Ara.HAP2) or *Tetrahymena thermophila* (T.HAP2). (B) shows levels of cell-cell fusion in cultures transfected with pcDNA alone, or vectors encoding the HAP2/GCS1 orthologs with or without co-transfection with plasmids encoding *Tetrahymena* GFU1, GFU2, or both (GFU1/2). Levels of cell-cell fusion were measured by counting the total number of nuclei in syncytia per field (y axis) in 4–6 random fields across 3 separate experiments. In each case, the midline represents the median, and the whiskers the minimum and maximum values for the total number of nuclei in syncytia per field, with a syncytium defined as any cell with ≥4 nuclei. In panels (A,B), statistical differences in pairwise comparisons between categories are indicated by horizontal lines above the plots as determined by Student's *t* test with asterisks denoting *p*-values (**** = $p < 0.0001$; ** = $p \leq 0.01$; * = $p \leq 0.05$; ns = not significant). In panel (B), asterisks above the categories represent statistical differences compared with the empty vector control calculated using a one-way, non-parametric Kruskal-Wallis ANOVA (**** = $p < 0.0001$; *** = $p \leq 0.001$).

Consistent with the work of Valansi et al.,[5] *Arabidopsis* HAP2/GCS1, by itself, drove moderate levels of cell-cell fusion relative to the positive control, in this case, Nipah virus G/F[54](Figure 4A). Similarly, as in previous work with *T. thermophila*,[3] expression of the ciliate ortholog in the absence of the other proteins induced some level of syncytia formation, although statistical significance was not achieved when compared to the negative control (vector alone) (Figure 4A). However, co-expression of *Tetrahymena* HAP2/GCS1 with either GFU1, GFU2, or both proteins resulted in about a 2-fold increase in mean activity, with syncytia formation reaching statistical significance in all cases (Figure 4B). While the combined effects were modest, no increase in activity was seen when GFU1 and GFU2 were co-expressed with *Arabidopsis* HAP2/GCS1 suggesting that species-specific interactions between the ciliate proteins may occur (Figure 4B).

Cooperativity between the fusion machinery on apposed membranes

While the precise interplay between HAP2/GCS1 and the newly described GFU1 and GFU2 proteins awaits further analysis, it was clear that both GFU1 and HAP2/GCS1 are required in both cells of a mating pair for efficient pore formation to occur (Figure 2I). This raised the interesting possibility that the fusion machinery on apposed membranes of mating cells somehow interact, an argument bolstered by the fact that the 75–85% decline in fusion efficiency observed when HAP2/GCS1 is deleted in one cell of a mating pair cannot be compensated for by high level expression of the native gene product in the wild type partner.[3,19]

To address this question further, we revisited the fusogenic capacity of transgenic cell lines carrying a mutation to a highly conserved arginine residue (R^{164}) that stabilizes the HAP2/GCS1 fusion loop(s) through formation of a salt bridge with an equally conserved glutamic acid residue (E^{108}) present in virtually all HAP2/GCS1 orthologs.[4] In previous studies with *Tetrahymena*, substitution of an alanine residue for the conserved arginine at position 164 had no effect on the ability of mutant cells to fuse with WT strains.[3] This was surprising since the same mutation abrogates the fusogenic capacity of HAP2/GCS1 in *Arabidopsis* and *Chlamydomonas* where the protein is present on only one gamete membrane.[4,7]

To determine whether the R^{164}A mutant protein was fully functional or whether the WT protein on the apposed membrane was able to rescue an otherwise defective gene product, we examined the ability of R^{164}A X R^{164}A mutant strains to form fusion pores using flow cytometry. As in previous studies,[3] reciprocal crosses between WT cells and cells carrying the mutant allele showed robust fusion (Figures 5A and 5C). However, pairs formed between R^{164}A mutant cell lines were completely unable to fuse (Figures 5B and 5C). These results support the involvement of R^{164} in the formation of a loop-stabilizing salt bridge and establish the importance of the loop structure

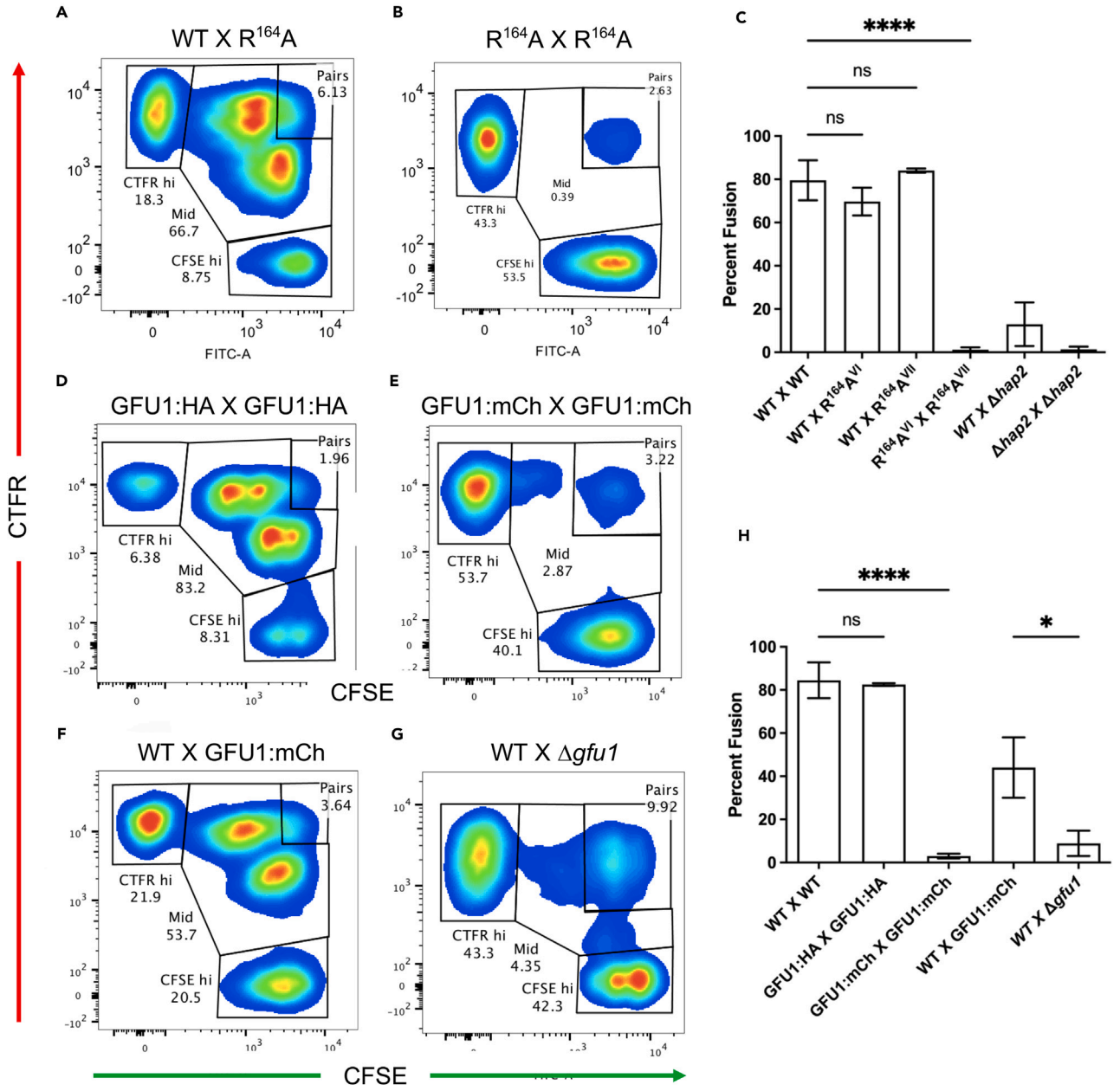

Figure 5. Cooperativity in membrane pore formation

(A) and (B) are representative flow cytometry plots of CFSE and CTFR-labeled cells expressing the $R^{164}A$ mutant allele of *HAP2/GCS1* mated to either WT cells (panel A) or a complementary mating type carrying the identical $R^{164}A$ mutant allele (panel B) fixed at 24 h post-mixing.

(C) is a bar graph showing the compiled data of percent fusion in crosses between WT, $R^{164}A$ mutant, and *Δhap2/gcs1* deletion strains as indicated on the x axis (n = 6–78 biological replicates/cross). The mating types (VI and VII) of strains carrying the $R^{164}A$ mutant allele are shown in superscript.

(D and E) are representative flow cytometry plots of crosses between CFSE and CTFR-labeled cells expressing C-terminal HA- or mCherry-tagged versions of GFU1, respectively, fixed at 24 h post-mixing. Fluorescence from the mCherry construct itself is negligible in fixed cells and does not contribute to the recorded signal.

(F and G), WT cells were mixed with either GFU1:mCherry expressing cells (F) or with a *Δgfu1* deletion strain lacking the gene (G), and fixed 24 h post-mixing. Note the substantially larger population of cells in the "Mid" gate in (F) compared to (G). Panel (H) is a bar graph showing the compiled data for percent fusion from all experiments with tagged GFU1 constructs (n = 3–18 biological replicates/cross). Bars in panels (C, H) represent the mean and bracketed lines the standard deviations (+/−). Asterisks represent the level of statistical significance between indicated crosses based on one-sided Kruskal-Wallis tests and Dunn's post-tests (**** = $p < 0.0001$; * = $p < 0.05$; ns = no significance).

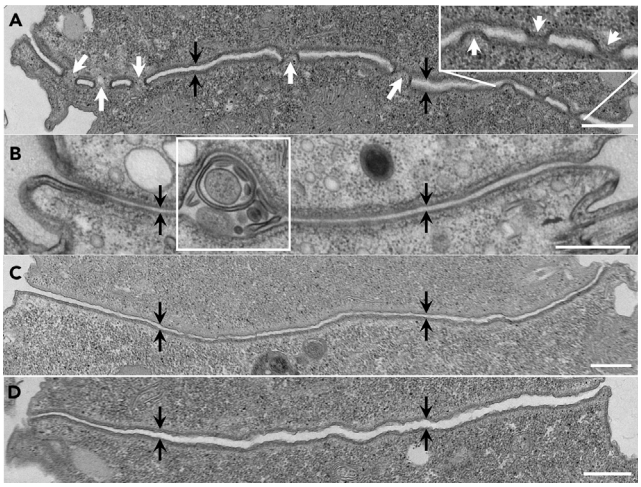

Figure 6. Ultrastructural analysis of membranes at the conjugation junction

Representative transmission electron micrographs showing sections spanning the conjugation junction of mating pairs are shown.

(A) = WT pair; panel (B) = Δ*hap2/gcs1* knockout pair; and panels (C) and (D) = Δ*gfu1* knockout pairs fixed at 4 h post-mixing. Cells are oriented top-to-bottom with the junctional membranes of each cell (demarcated by small black arrows) running horizontally at the middle of each panel. In panel (A), numerous pores (white arrows) were visible along the length of the conjugation junction in the WT pair. The inset at the upper right is a higher magnification image showing dome-shaped structures (white arrows) that appeared to push membranes outward toward the apposed membrane. In serial sections, these structures were shown to be fully open pores cut at an oblique angle (Figure S5). In (B), no pores were visible along the junctional membranes formed by Δ*hap2/gcs1* deletion strains. However, large vesicular bodies (bordered by the white square) were present in the luminal space separating cells.

In (C) and (D), neither junctional pores nor large vesicular bodies were visible in pairs formed by Δ*gfu1* deletion strains. Note the slightly greater distance between cells in (D) compared to (C). Scale bars in the lower right corner of each panel = 0.5 μm.

for HAP2/GCS1-mediated fusion of *Tetrahymena* mating types. More importantly, the ability of the WT protein to rescue the $R^{164}A$ mutation provides further evidence for potential interactions between the fusion machinery on apposed membranes of mating cells.

While such interactions may be possible in the case of HAP2/GCS1, GFU1 is almost certainly not a transmembrane protein and therefore should be incapable of interacting either with itself or other proteins across the *trans*-junctional space. Nevertheless, evidence of cooperativity involving GFU1 was uncovered in studies to validate the functionality of HA- and mCherry-tagged versions of the protein. As determined by flow cytometry, cells expressing HA-tagged GFU1 showed WT levels of fusion when mated to each other indicating that the tagged protein was fully functional (Figures 5D and 5H). By contrast, cells expressing the mCherry-tagged version underwent very low levels of fusion (<3% of cells) indicating that the larger tag rendered GFU1 inactive (Figures 5E and 5H). However, when crossed to WT cells, transgenic cells expressing the GFU1:mCherry chimera underwent ~50% fusion (Figures 5F and 5H), significantly more than that seen in crosses between WT cells and *Δgfu1* knockout strains (Figures 5G and 5H). As with the $R^{164}A$ mutation of HAP2/GCS1, the substantial rescue of an otherwise defective mCherry-tagged version of GFU1 by the WT gene product on partnering cells would clearly suggest that cooperative interactions are at play between apposed membranes of mating cells.

Membrane architecture in the absence of GFU1

Given its localization at the conjugation junction, its predicted BAR-like domain structure, and its ability to interact with model membranes (Figure 3), it was tempting to speculate that GFU1 plays a role in membrane remodeling events leading up to membrane pore opening in mating cells. To examine this, we performed ultrastructural studies on mating pairs formed by WT, *Δhap2/gcs1*, and *Δgfu1* deletion strains.

WT X WT pairs fixed 2–4 h post-mixing showed normal morphology with closely apposed membranes interrupted by numerous pores along the length of the conjugation junction (Figure 6A). In addition to open pores, broad dome-shaped protrusions were seen along junctional membranes that, in serial section, were revealed to be fully open pores cut at an oblique angle (Figure S5).

Within the same time frame, Δ*hap2/gcs1* X Δ*hap2/gcs1* pairs also showed closely apposed membranes but unlike WT pairs, were completely devoid of junctional pores (Figure 6B). Instead, large membrane vesicles/tubules were frequently observed in the luminal space separating *Δhap2/Δgcs1* knockout pairs (Figure 6B) as previously reported.[24]

Lastly, pairs formed by *Δgfu1* deletion strains appeared similar to *Δhap2/gcs1* X *Δhap2/gcs1* pairs but showed interesting differences as well. Like Δ*hap2/gcs1* pairs, *Δgfu1* pairs showed a complete absence of junctional pores (Figures 6C and 6D). However, in >100 pairs examined, large extracellular vesicles were never observed in the junctional space between cells, a marked difference with the *Δhap2/gcs1* knockout pairs. Additionally, *Δgfu1* pairs showed greater variability in the distances between cells (Figures 6C and 6D) and the occasional presence of cilia within the junctional space (not shown).

DISCUSSION

As shown here, *Tetrahymena* mating types carrying deletions in either *GFU1* or *GFU2* were able to recognize and adhere to their complimentary deletion strains, but, as in the case of Δ*hap2/gcs1* knockouts, were unable to form fusion pores. The corresponding GFU1 and GFU2 gene products can therefore be added to a list of lineage-specific factors, that together with MAR1 in *Chlamydomonas reinhardtii*,[15] and the DMP8/9 proteins of *Arabidopsis thaliana*, regulate HAP2/GCS1-mediated gamete merger during fertilization.

From a functional standpoint, MAR1 and the DMP8/9 proteins play critical roles in the localization and timely activation of HAP2/GCS1 in algae and plants, respectively.[15,17,55,56] Whether the same is true of the newly identified GFU1 and GFU2 proteins is unclear. GFU1 contains neither a signal peptide nor transmembrane helices and is therefore likely to be entirely intracellular. However, its predicted structural resemblance to BAR-domains and ability to interact with model membranes is intriguing from a functional standpoint. As discussed below, BAR-domain containing proteins have been shown to alter membrane structure in a variety of ways, and the bilateral requirement for FUS7/Rvs161 in successful mating in *Saccharomyces* establishes a role for these proteins in fertilization, at least in fungi.

Unlike GFU1, GFU2 is a single-pass transmembrane protein that would presumably be free to bind receptors on the apposed membranes of mating cells. Indeed, given the reduced kinetics of pairing in crosses between complementary Δ*gfu2* deletion strains (Figure 1F), GFU2 could act in gamete recognition and adherence, or participate in activation of the HAP2/GCS1 fusion machinery as a member of a hypothetical receptor-ligand pair or signaling complex. That said, it is unlikely that GFU2 interacts directly with HAP2/GCS1 as may be the case for DMP8/9,[17] and possibly MAR1[15] as well. If such interactions occur, one would expect that the absence of GFU2 in one cell of a mating pair would have a significant impact on HAP2/GCS1-mediated fusion in *T. thermophila*, which is clearly not the case (Figures 2H and 2I).

While additional work is needed to define the precise roles GFU1 and GFU2, evidence of cooperativity between the fusion machinery on mating cells raises important questions regarding the underlying mechanisms of HAP2/GCS1-mediated gamete fusion, not just in *Tetrahymena* but in sexually dichotomous species such as *Arabidopsis thaliana*, where the protein is limited to the surfaces of male gametes.

In *Arabidopsis*, HAP2/GCS1 drives gamete fusion from a single membrane. Nevertheless, in mammalian cells, syncytia formation occurs only when the plant ortholog is expressed on the membranes of adjacent cells.[5] While this unusual bilateral requirement in a heterologous system may reflect an absence of cellular factors that ordinarily facilitate gamete fusion in *A. thaliana*, the developmental fusion proteins AFF-1 and EFF-1 have a similar bilateral requirement for syncytia formation, both in worm tissues and following heterologous expression in cultured insect cells.[29,30] As noted earlier, AFF-1 and EFF-1 are structurally homologous to class II viral fusogens, although EFF-1 is thought to lack a hydrophobic fusion loop.[34] To account for these bilateral requirements and the ability of EFF-1 to catalyze syncytia formation in the absence of an obvious fusion loop, models involving homotypic *trans*-interactions between protomers[32,34] or between fully formed trimers on apposed membranes have been proposed.[35]

To our knowledge, there is little direct evidence to support such models. Nevertheless, homotypic *trans*-interactions could explain the bilateral requirement for HAP2/GCS1 in *Tetrahymena*, with the caveat that HAP2/GCS1-mediated gamete fusion requires functional fusion loops.[3,8,9] A model involving fusion loop insertion and trimerization of protomers emanating from apposed membranes of mating cells is shown in Figure 7A. Considering the data presented here, this model has several major drawbacks. First and foremost, it predicts that in *Tetrahymena*, trimers formed through interactions in trans would be more efficient than trimers emanating from a single membrane (otherwise, WT X Δ*hap2/gcs1* pairs would fuse efficiently). Given the high degree of conservation in HAP2/GCS1 structure and the ability of the protein to act unilaterally from a single membrane in other species, this seems unlikely. Second, based on steric considerations, it is unclear whether promoters that span membranes in the opposite orientation would be capable of forming mixed trimers. Lastly, given the importance of the fusion loops for HAP2/GCS1 trimerization,[8,9] it is unlikely that R^{164}A mutant protomers could form *trans*-trimers with the native protein on the apposed membrane regardless of steric considerations.

Given these drawbacks, alternative models of cooperativity must be considered. A model that we currently favor is shown in Figures 7B–7F. In this scenario, rather than homotypic *trans*-interactions between proteins, interactions between curved membrane structures destabilized by HAP2/GCS1 would be required for efficient fusion. As with conventional models, fusion pore opening would necessitate the formation of HAP2/GCS1 trimers from monomers/dimers on the same membrane (Figures 7B–7D), but conformational foldback alone would be insufficient to drive membrane pore opening and/or expansion. Rather, the critical threshold for fusion would only be met where curved membrane structures destabilized by HAP2/GCS1 interact. In this case, membrane curvature would be imposed by the HAP2/GCS1 transmembrane helix and cytosolic domain in concert with other proteins such as GFU1.

Such a scenario could explain the ability of the native protein to rescue membrane pore formation in cells carrying the R^{164}A mutation (Figures 7C and 7D), as well as the low level of fusion seen with Δ*hap2/gcs1* deletion strains (Figure 7E). In the first instance, so long as the mutant protein imparts local curvature to the membrane of one cell and the native protein both curvature and the ability to form functional trimers in the other (Figures 7C and 7D), fusion pores would form at sites where unstable regions of the membrane interact. With Δ*hap2/gcs1* deletion strains however, the energy barrier to membrane merger would be difficult to overcome in the absence of curved or destabilized membrane structures on one or both cells of a mating pair (Figures 7E and 7F, respectively). An important corollary to this argument would be that species in which HAP2/GCS1 is expressed in only one gamete (*A. thaliana*, *C. reinhardtii*, *etc.*) would still require curved or destabilized membrane structures on both cells of a mating pair but would resort to other proteins to accomplish this in the gamete lacking HAP2/GCS1.

While purely speculative, there is clear evidence for the involvement of specialized membrane structures in a variety of cell-cell fusion events including fertilization. In *Chlamydomonas*, for example, gamete fusion is initiated at the distal tips of microvillar-like protrusions on *plus* and *minus* mating types where membrane curvature is high. Along the same lines, actin-dependent invasive protrusions have been

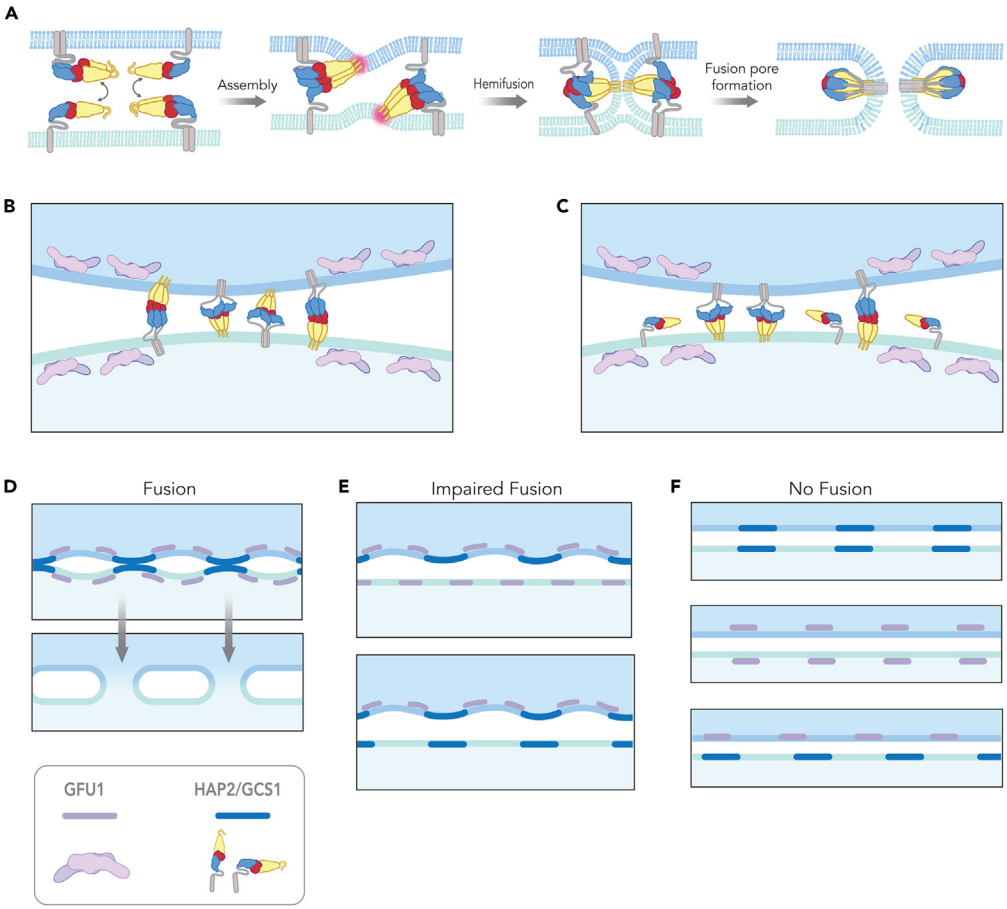

Figure 7. Alterative models of cooperativity in the fusion process

(A and B) Like previous models proposed for EFF-1 from *C. elegans*,[32,34] the model shown in panel (A) hypothesizes that HAP2/GCS1 protomers emanating from apposed membranes on either side of the conjugation junction interact to form trimers, except that in this case, insertion of fusion loops into lipid bilayers would be obligatory. As in conventional models for class II viral fusogens, trimers would then undergo conformational foldback to generate the forces necessary to bend membranes and promote fusion pore opening. Alternatively, the model in panel (B) forgoes *trans*-interactions between the HAP2/GCS1 protomers and proposes instead that the HAP2/GCS1 transmembrane helix and cytosolic domains together with other proteins such as GFU1, impose local membrane curvature creating an energetically favorable environment for membrane fusion where such regions interact.

(C) depicts a scenario in which the R^{164}A mutant protein in the lower bilayer would be unable to form trimers but would still deform the membrane and lower the energy barrier for membrane merger catalyzed by native HAP2/GCS1 trimers on the apposed membrane.

(D) shows the expected outcome for crosses between WT cells or WT X R^{164}A strains, namely full fusion where curved membranes interact.

(E) shows the expected outcome when either HAP2/GCS1 or GFU1 are absent from one membrane, namely, inefficient fusion of only a small percentage of pairs.

(F) shows the expected outcome when either HAP2/GCS1 or GFU1 are absent from both membranes (upper two schematics) or in crosses between cells lacking one or the other protein (lower schematic), namely, no fusion.

shown to enhance bilateral EFF-1 dependent syncytia formation in cultured insect cells.[57] Indeed, the involvement of microvilli and other membrane protrusions in cell-cell fusion, as well as virus-host-cell fusion has long been argued.[58–61] From a mechanistic standpoint, such protrusions could lower the energy barrier to fusion pore opening by forcing the outer leaflets of apposed membranes into close proximity. Alternatively (or in addition), curved membranes associated with these structures could provide an energetically favorable environment for lipid mixing following conformational foldback of HAP2/GCS1 trimers.

In either case, the involvement of BAR-domain containing proteins in promoting membrane curvature and the formation of filopodia, lamellipodia, and related membrane protrusions in other cell types[37,38,62,63] would suggest a possible role for GFU1 in this scenario as well (Figures 7B–7F). Importantly, BAR-domain containing proteins have been linked to cell-cell fusion events in at least two instances, namely, fertilization in yeast where there is a bilateral requirement for FUS7/Rvs161 in mating of *S. cerevisiae*,[64,65] and during virus-induced syncytia formation where elevated levels of BAR-domain fragments have been shown to promote fusion of cultured cells by influenza HA and baculovirus gp64, through effects on pore expansion.[66]

Although previous studies in *Tetrahymena*[23] have correlated the presence of microvillar-like protrusions with sites of membrane pore opening at the conjugation junction, we were unable to identify such structures in the present study presumably owing to their small size

and transient nature. Thus, we were unable to assign roles for HAP2/GCS1 or GFU1 in their formation. Nevertheless, the presence of large membrane vesicles/tubules within the luminal space separating Δ*hap2/gcs1* deletion strains raises interesting questions regarding a possible role of HAP2/GCS1 in membrane sculpting. While the absence of such vesicles in the Δ*gfu1* knockout crosses could be interpreted in the same way, additional studies will be required to validate what role these proteins have in membrane curvature or the formation of membrane protrusions, if any. Indeed, in the case of GFU1, variability in the distances between mating cells seen in the Δ*gfu1* knockout pairs (Figures 6C and 6D) could suggest an entirely different role for this protein, for example, in ensuring close cell-cell adherence and/or the ability of cells to maintain open pores rather than in membrane curvature per se.

Finally, apart from mechanistic considerations, the requirement for HAP2/GCS1 expression in all mating types of *T. thermophila* has additional implications both in evolutionary terms, and for fertilization success in organisms with multiple mating types. In the first instance, ubiquitous expression of an otherwise "male" gamete-specific gene product in *Tetrahymena* may reflect the vestiges of an early isogametic lifestyle in which the expression of "male" and "female" genes were not yet restricted to a given mating type.[24,36] If this is indeed the case, cooperativity between the HAP2/GCS1 fusion machinery on the apposed membranes of mating cells may represent the evolutionary ground state. In that case, restricted expression of HAP2/GCS1 to a single (predominantly male) gamete in sexually dichotomous species would have required either the emergence of other proteins to compensate for its absence on the membranes of partnering cells, or a change in HAP2/GCS1 structure allowing it to function more efficiently from a single membrane.

On the second point, in species with more than three mating types, fertilization would be haphazard if not all mating types express the fusogen. For example, in *T. thermophila*, mating type recognition and adherence occur even in the absence of HAP2/GCS1 presumably due to proteins encoded at the mating type locus[21,67] and elsewhere in the macronuclear genome. Furthermore, fertilization succeeds (albeit inefficiently) as long as one cell expresses the fusogen. However, if two or more mating types failed to express HAP2/GCS1, some pairs would be unable to exchange pronuclei, thus undermining any potential benefit of a multiple mating type system.

Limitations of the study

The models proposed in Figure 7 are attempts to explain the bilateral requirements for HAP2/GCS1 activity in *Tetrahymena* shown here and elsewhere,[3] but remain strictly theoretical in the absence of direct evidence. While we are less inclined to believe the first model (Figure 7A) for reasons indicated in the text, efforts to demonstrate direct *trans*-interactions between HAP2/GCS1 protomers on apposed membranes were unsuccessful in our hands using a co-immunoprecipitation approach. Specifically, in preliminary work we found that N-terminal tags on HAP2/GCS1 interfered with its function and C-terminal tags were proteolytically cleaved from the protein either before or during purification. This precluded attempts to show both homotypic *trans*-interactions as well as potential interactions between HAP2/GCS1 and the novel proteins, GFU1 and GFU2. By the same token, while we favor the model shown in Figures 7B–7F, we were unable to visualize membrane protrusions or other obvious curved membrane structures in wild type or mutant cell lines using conventional transmission electron microscopy and were unable to demonstrate an association of HAP2 or GFU1 with such structures using low-resolution fluorescence light microscopy.

STAR★METHODS

Detailed methods are provided in the online version of this paper and include the following:

- KEY RESOURCES TABLE
- RESOURCE AVAILABILITY
  - Lead contact
  - Materials availability
  - Data and code availability
- EXPERIMENTAL MODEL AND STUDY PARTICIPANT DETAILS
  - Growth of Tetrahymena thermophila strains
- METHOD DETAILS
  - Mating of Tetrahymena strains
  - Construction of *GFU1* and *GFU2* deletion strains
  - Construction of mutant strains
  - Δ*hap2/gcs1* deletion strains
  - Pair stability assays
  - Flow cytometric fusion assays
  - Fusion assays in mammalian cell culture
  - Fluorescence microscopy
  - Isolation of recombinant GFU1
  - Lipid ESR assays
  - Fluorescence dequenching assay
  - Ultrastructural studies
  - Protein structure modeling
- QUANTIFICATION AND STATISTICAL ANALYSIS

SUPPLEMENTAL INFORMATION

Supplemental information can be found online at https://doi.org/10.1016/j.isci.2024.110146.

ACKNOWLEDGMENTS

We thank Mozammal Hossain and Catherine Devine for their excellent technical assistance in growth and maintenance of *Tetrahymena* strains. We also thank James Cockey for assistance with flow cytometry experiments, as well as Alyanis Acedo Serruno, Anita Liu, and Abbey Robinson for assistance in cloning the GFU1 gene in *E. coli*. The research reported in this publication was supported by awards from the National Institutes of Health (NIH) to T.G.C. (P40 award OD010964-18; Office of Research Infrastructure Programs), and to H.C.A. (R01 award AI104092; National Institute of Allergy and Infectious Diseases), and from the National Science Foundation (NSF) to E.S.C. (award #1947608). Biophysical studies were conducted at the National Center for Advanced Electron-Spin Resonance Spectroscopy (ACERT) with funding from the NIH (awards to J.H.F. R24GM146107 for ACERT, and R35GM148272 for protein/membrane interaction). Additional support was awarded to J.F.P. in the form of an NSF Graduate Research Fellowship (DGE-1144153) and an NIH K99GM146112 award. Any opinions, findings, and conclusions expressed in this manuscript are those of the authors and do not necessarily reflect the views of the NIH or NSF. Finally, we thank the National Tetrahymena Stock Center for providing *T. thermophila* strains.

AUTHOR CONTRIBUTIONS

Conceptualization, T.G.C., J.L., J.F.P., and F.A.R.; Methodology, T.G.C., J.L., J.F.P., J.L., F.A.R., and L.L.; Supervision, T.G.C., D.C.-H., J.H.F., and H.C.A.; Investigation, J.F.P., J.L., E.S.S., D.K., A.A., R.A., N.J.N., Y.B., H.P., H.M.B., E.S.C., L.L., and T.M.; Writing – Original Draft, T.G.C. and J.F.P.; Writing – Review and Editing, J.L., J.F.P., E.S.S., H.B., E.S.C., D.C.-H., H.C.A., F.A.R., and L.L.; Visualization, J.F.P., E.S.S., H.B., F.A.R., and T.G.C.; Formal Analysis, J.F.P., H.B., H.C.A., L.L., and E.S.S.; Project Administration, T.G.C., D.C.-H., J.H.F., J.L., and L.L.; Funding Acquisition, T.G.C., J.L., J.F.P., E.S.C., H.C.A., F.A.R., and J.H.F.

DECLARATION OF INTERESTS

The authors declare no competing interests.

Received: May 29, 2023
Revised: April 29, 2024
Accepted: May 27, 2024
Published: May 28, 2024

REFERENCES

1. Wong, J.L., and Johnson, M.A. (2010). Is HAP2-GCS1 an ancestral gamete fusogen? Trends Cell Biol. *20*, 134–141. https://doi.org/10.1016/j.tcb.2009.12.007.
2. Speijer, D., Lukeš, J., and Eliáš, M. (2015). Sex is a ubiquitous, ancient, and inherent attribute of eukaryotic life. Proc. Natl. Acad. Sci. USA *112*, 8827–8834. https://doi.org/10.1073/pnas.1501725112.
3. Pinello, J.F., Lai, A.L., Millet, J.K., Cassidy-Hanley, D., Freed, J.H., and Clark, T.G. (2017). Structure-Function Studies Link Class II Viral Fusogens with the Ancestral Gamete Fusion Protein HAP2. Curr. Biol. *27*, 651–660. https://doi.org/10.1016/j.cub.2017.01.049.
4. Fédry, J., Liu, Y., Péhau-Arnaudet, G., Pei, J., Li, W., Tortorici, M.A., Traincard, F., Meola, A., Bricogne, G., Grishin, N.V., et al. (2017). The Ancient Gamete Fusogen HAP2 Is a Eukaryotic Class II Fusion Protein. Cell *168*, 904–915.e10. https://doi.org/10.1016/j.cell.2017.01.024.
5. Valansi, C., Moi, D., Leikina, E., Matveev, E., Graña, M., Chernomordik, L.V., Romero, H., Aguilar, P.S., and Podbilewicz, B. (2017). Arabidopsis HAP2/GCS1 is a gamete fusion protein homologous to somatic and viral fusogens. J. Cell Biol. *216*, 571–581. https://doi.org/10.1083/jcb.201610093.
6. Baquero, E., Fedry, J., Legrand, P., Krey, T., and Rey, F.A. (2019). Species-Specific Functional Regions of the Green Alga Gamete Fusion Protein HAP2 Revealed by Structural Studies. Structure *27*, 113–124.e4. https://doi.org/10.1016/j.str.2018.09.014.
7. Fedry, J., Forcina, J., Legrand, P., Péhau-Arnaudet, G., Haouz, A., Johnson, M., Rey, F.A., and Krey, T. (2018). Evolutionary diversification of the HAP2 membrane insertion motifs to drive gamete fusion across eukaryotes. PLoS Biol. *16*, e2006357. https://doi.org/10.1371/journal.pbio.2006357.
8. Zhang, J., Pinello, J.F., Fernández, I., Baquero, E., Fedry, J., Rey, F.A., and Snell, W.J. (2021). Species-specific gamete recognition initiates fusion-driving trimer formation by conserved fusogen HAP2. Nat. Commun. *12*, 4380. https://doi.org/10.1038/s41467-021-24613-8.
9. Feng, J., Dong, X., Su, Y., Lu, C., and Springer, T.A. (2022). Monomeric prefusion structure of an extremophile gamete fusogen and stepwise formation of the postfusion trimeric state. Nat. Commun. *13*, 4064. https://doi.org/10.1038/s41467-022-31744-z.
10. Angrisano, F., Sala, K.A., Da, D.F., Liu, Y., Pei, J., Grishin, N.V., Snell, W.J., and Blagborough, A.M. (2017). Targeting the Conserved Fusion Loop of HAP2 Inhibits the Transmission of Plasmodium berghei and falciparum. Cell Rep. *21*, 2868–2878. https://doi.org/10.1016/j.celrep.2017.11.024.
11. Feng, J., Dong, X., Pinello, J., Zhang, J., Lu, C., Iacob, R.E., Engen, J.R., Snell, W.J., and Springer, T.A. (2018). Fusion surface structure, function, and dynamics of gamete fusogen HAP2. Elife *7*, e39772. https://doi.org/10.7554/eLife.39772.
12. Kielian, M. (2014). Mechanisms of Virus Membrane Fusion Proteins. Annu. Rev. Virol. *1*, 171–189. https://doi.org/10.1146/annurev-virology-031413-085521.
13. Guardado-Calvo, P., and Rey, F.A. (2021). The Viral Class II Membrane Fusion Machinery: Divergent Evolution from an Ancestral Heterodimer. Viruses *13*, 2368. https://doi.org/10.3390/v13122368.
14. Leikina, E., Gamage, D.G., Prasad, V., Goykhberg, J., Crowe, M., Diao, J., Kozlov, M.M., Chernomordik, L.V., and Millay, D.P. (2018). Myomaker and Myomerger Work Independently to Control Distinct Steps of Membrane Remodeling during Myoblast Fusion. Dev. Cell *46*, 767–780.e7. https://doi.org/10.1016/j.devcel.2018.08.006.
15. Pinello, J.F., Liu, Y., and Snell, W.J. (2021). MAR1 links membrane adhesion to membrane merger during cell-cell fusion in Chlamydomonas. Dev. Cell *56*, 3380–3392.e9. https://doi.org/10.1016/j.devcel.2021.10.023.
16. Liu, Y., Tewari, R., Ning, J., Blagborough, A.M., Garbom, S., Pei, J., Grishin, N.V., Steele, R.E., Sinden, R.E., Snell, W.J., and Billker, O. (2008). The conserved plant sterility gene HAP2 functions after attachment of fusogenic membranes in Chlamydomonas and Plasmodium gametes. Genes Dev. *22*, 1051–1068.

17. Wang, W., Xiong, H., Zhao, P., Peng, X., Sun, M.X., Zhao, P., Peng, X., Sprunck, S., and Sun, M.-X. (2022). DMP8 and 9 regulate HAP2/GCS1 trafficking for the timely acquisition of sperm fusion competence. Proc. Natl. Acad. Sci. USA *119*. e2207608119. https://doi.org/10.1073/pnas.2207608119.
18. Sprunck, S., Rademacher, S., Vogler, F., Gheyselinck, J., Grossniklaus, U., and Dresselhaus, T. (2012). Egg cell-secreted EC1 triggers sperm cell activation during double fertilization. Science (New York, N.Y.) *338*, 1093–1097.
19. Pinello, J.F., and Clark, T.G. (2021). HAP2-Mediated Gamete Fusion: Lessons From the World of Unicellular Eukaryotes. Front. Cell Dev. Biol. *9*, 807313. https://doi.org/10.3389/fcell.2021.807313.
20. Cole, E., and Sugai, T. (2012). Developmental progression of Tetrahymena through the cell cycle and conjugation. Methods Cell Biol. *109*, 177–236.
21. Cervantes, M.D., Hamilton, E.P., Xiong, J., Lawson, M.J., Yuan, D., Hadjithomas, M., Miao, W., and Orias, E. (2013). Selecting one of several mating types through gene segment joining and deletion in Tetrahymena thermophila. PLoS Biol. *11*, e1001518. https://doi.org/10.1371/journal.pbio.1001518.
22. Cole, E.S. (2006). The Tetrahymena Conjugation Junction. In Cell-Cell Channels (Springer), pp. 39–62. https://doi.org/10.1007/978-0-387-46957-7_3.
23. Cole, E.S., Giddings, T.H., Ozzello, C., Winey, M., O'Toole, E., Orias, J., Hamilton, E., Guerrier, S., Ballard, A., and Aronstein, T. (2015). Membrane dynamics at the nuclear exchange junction during early mating (one to four hours) in the ciliate Tetrahymena thermophila. Eukaryot. Cell *14*, 116–127. https://doi.org/10.1128/EC.00164-14.
24. Cole, E.S., Cassidy-Hanley, D., Fricke Pinello, J., Zeng, H., Hsueh, M., Kolbin, D., Ozzello, C., Giddings, T., Jr., Winey, M., and Clark, T.G. (2014). Function of the male-gamete-specific fusion protein HAP2 in a seven-sexed ciliate. Curr. Biol. *24*, 2168–2173.
25. Orias, J.D., Hamilton, E.P., and Orias, E. (1983). A microtubule meshwork associated with gametic pronucleus transfer across a cell-cell junction. Science *222*, 181–184. https://doi.org/10.1126/science.6623070.
26. Steele, R.E., and Dana, C.E. (2009). Evolutionary History of the HAP2/GCS1 Gene and Sexual Reproduction in Metazoans. PLoS One *4*, e7680. https://doi.org/10.1371/journal.pone.0007680.
27. Mori, T., Kuroiwa, H., Higashiyama, T., and Kuroiwa, T. (2006). GENERATIVE CELL SPECIFIC 1 is essential for angiosperm fertilization. Nat. Cell Biol. *8*, 64–71.
28. Iosilevskii, Y., and Podbilewicz, B. (2021). Programmed cell fusion in development and homeostasis. In Current Topics in Developmental Biology (Elsevier), pp. 215–244. https://doi.org/10.1016/bs.ctdb.2020.12.013.
29. Sapir, A., Choi, J., Leikina, E., Avinoam, O., Valansi, C., Chernomordik, L.V., Newman, A.P., and Podbilewicz, B. (2007). AFF-1, a FOS-1-Regulated Fusogen, Mediates Fusion of the Anchor Cell in C. elegans. Dev. Cell *12*, 683–698. https://doi.org/10.1016/j.devcel.2007.03.003.
30. Podbilewicz, B., Leikina, E., Sapir, A., Valansi, C., Suissa, M., Shemer, G., and Chernomordik, L.V. (2006). The C. elegans Developmental Fusogen EFF-1 Mediates Homotypic Fusion in Heterologous Cells and In Vivo. Dev. Cell *11*, 471–481. https://doi.org/10.1016/j.devcel.2006.09.004.
31. von Besser, K., Frank, A.C., Johnson, M.A., and Preuss, D. (2006). Arabidopsis HAP2 (GCS1) is a sperm-specific gene required for pollen tube guidance and fertilization. Development (Cambridge, England) *133*, 4761–4769.
32. Zeev-Ben-Mordehai, T., Vasishtan, D., Siebert, C.A., and Grünewald, K. (2014). The full-length cell–cell fusogen EFF-1 is monomeric and upright on the membrane. Nat. Commun. *5*, 3912. https://doi.org/10.1038/ncomms4912.
33. Hernández, J.M., and Podbilewicz, B. (2017). The hallmarks of cell-cell fusion. Development *144*, 4481–4495. https://doi.org/10.1242/dev.155523.
34. Perez-Vargas, J., Krey, T., Valansi, C., Avinoam, O., Haouz, A., Jamin, M., Raveh-Barak, H., Podbilewicz, B., and Rey, F.A. (2014). Structural basis of eukaryotic cell-cell fusion. Cell *157*, 407–419.
35. Podbilewicz, B. (2014). Virus and Cell Fusion Mechanisms. Annu. Rev. Cell Dev. Biol. *30*, 111–139. https://doi.org/10.1146/annurev-cellbio-101512-122422.
36. Orias, E. (2014). Membrane fusion: HAP2 protein on a short leash. Curr. Biol. *24*, R831–R833. https://doi.org/10.1016/j.cub.2014.08.004.
37. Simunovic, M., Evergren, E., Callan-Jones, A., and Bassereau, P. (2019). Curving Cells Inside and Out: Roles of BAR Domain Proteins in Membrane Shaping and Its Cellular Implications. Annu. Rev. Cell Dev. Biol. *35*, 111–129. https://doi.org/10.1146/annurev-cellbio-100617-060558.
38. Peter, B.J., Kent, H.M., Mills, I.G., Vallis, Y., Butler, P.J.G., Evans, P.R., and McMahon, H.T. (2004). BAR domains as sensors of membrane curvature: the amphiphysin BAR structure. Science *303*, 495–499. https://doi.org/10.1126/science.1092586.
39. Xiong, J., Lu, Y., Feng, J., Yuan, D., Tian, M., Chang, Y., Fu, C., Wang, G., Zeng, H., and Miao, W. (2013). Tetrahymena functional genomics database (TetraFGD): an integrated resource for Tetrahymena functional genomics. Database *2013*, bat008. https://doi.org/10.1093/database/bat008.
40. Loidl, J. (2021). Tetrahymena meiosis: Simple yet ingenious. PLoS Genet. *17*, e1009627. https://doi.org/10.1371/journal.pgen.1009627.
41. Akematsu, T., Sánchez-Fernández, R., Kosta, F., Holzer, E., and Loidl, J. (2020). The Transmembrane Protein Semi1 Positions Gamete Nuclei for Reciprocal Fertilization in Tetrahymena. iScience *23*, 100749. https://doi.org/10.1016/j.isci.2019.100749.
42. Wang, S., Li, W., Liu, S., and Xu, J. (2016). RaptorX-Property: a web server for protein structure property prediction. Nucleic Acids Res. *44*, W430–W435. https://doi.org/10.1093/nar/gkw306.
43. Moravcevic, K., Alvarado, D., Schmitz, K.R., Kenniston, J.A., Mendrola, J.M., Ferguson, K.M., and Lemmon, M.A. (2015). Comparison of Saccharomyces cerevisiae F-BAR Domain Structures Reveals a Conserved Inositol Phosphate Binding Site. Structure *23*, 352–363. https://doi.org/10.1016/j.str.2014.12.009.
44. Shimada, A., Takano, K., Shirouzu, M., Hanawa-Suetsugu, K., Terada, T., Toyooka, K., Umehara, T., Yamamoto, M., Yokoyama, S., and Suetsugu, S. (2010). Mapping of the basic amino-acid residues responsible for tubulation and cellular protrusion by the EFC/F-BAR domain of pacsin2/Syndapin II. FEBS Lett. *584*, 1111–1118. https://doi.org/10.1016/j.febslet.2010.02.058.
45. McDonald, N.A., Takizawa, Y., Feoktistova, A., Xu, P., Ohi, M.D., Vander Kooi, C.W., and Gould, K.L. (2016). The Tubulation Activity of a Fission Yeast F-BAR Protein Is Dispensable for Its Function in Cytokinesis. Cell Rep. *14*, 534–546. https://doi.org/10.1016/j.celrep.2015.12.062.
46. Jumper, J., Evans, R., Pritzel, A., Green, T., Figurnov, M., Ronneberger, O., Tunyasuvunakool, K., Bates, R., Žídek, A., Potapenko, A., et al. (2021). Highly accurate protein structure prediction with AlphaFold. Nature *596*, 583–589. https://doi.org/10.1038/s41586-021-03819-2.
47. wwPDB consortium, Burley, S.K., Berman, H.M., Bhikadiya, C., Bi, C., Chen, L., Costanzo, L.D., Christie, C., Duarte, J.M., Dutta, S., et al. (2019). Protein Data Bank: the single global archive for 3D macromolecular structure data. Nucleic Acids Res. *47*, D520–D528. https://doi.org/10.1093/nar/gky949.
48. Ge, M., and Freed, J.H. (2009). Fusion Peptide from Influenza Hemagglutinin Increases Membrane Surface Order: An Electron-Spin Resonance Study. Biophys. J. *96*, 4925–4934. https://doi.org/10.1016/j.bpj.2009.04.015.
49. Lai, A.L., and Freed, J.H. (2015). The Interaction between Influenza HA Fusion Peptide and Transmembrane Domain Affects Membrane Structure. Biophys. J. *109*, 2523–2536. https://doi.org/10.1016/j.bpj.2015.10.044.
50. Boucrot, E., Pick, A., Çamdere, G., Liska, N., Evergren, E., McMahon, H.T., and Kozlov, M.M. (2012). Membrane Fission Is Promoted by Insertion of Amphipathic Helices and Is Restricted by Crescent BAR Domains. Cell *149*, 124–136. https://doi.org/10.1016/j.cell.2012.01.047.
51. Rawling, J., Cano, O., Garcin, D., Kolakofsky, D., and Melero, J.A. (2011). Recombinant Sendai Viruses Expressing Fusion Proteins with Two Furin Cleavage Sites Mimic the Syncytial and Receptor-Independent Infection Properties of Respiratory Syncytial Virus. J. Virol. *85*, 2771–2780. https://doi.org/10.1128/JVI.02065-10.
52. Stanifer, M.L., Cureton, D.K., and Whelan, S.P.J. (2011). A Recombinant Vesicular Stomatitis Virus Bearing a Lethal Mutation in the Glycoprotein Gene Uncovers a Second Site Suppressor That Restores Fusion. J. Virol. *85*, 8105–8115. https://doi.org/10.1128/JVI.00735-11.
53. González-Reyes, L., Ruiz-Argüello, M.B., García-Barreno, B., Calder, L., López, J.A., Albar, J.P., Skehel, J.J., Wiley, D.C., and Melero, J.A. (2001). Cleavage of the human respiratory syncytial virus fusion protein at two distinct sites is required for activation of membrane fusion. Proc. Natl. Acad. Sci. USA *98*, 9859–9864. https://doi.org/10.1073/pnas.151098198.
54. Contreras, E.M., Johnston, G.P., Buchholz, D.W., Ortega, V., Monreal, I.A., Zamora, J.L.R., Cheung, T., and Aguilar, H.C. (2021). Roles of Cholesterol in Early and Late Steps of the Nipah Virus Membrane Fusion Cascade. J. Virol. *95*. e02323-20. https://doi.org/10.1128/JVI.02323-20.
55. Cyprys, P., Lindemeier, M., and Sprunck, S. (2019). Gamete fusion is facilitated by two sperm cell-expressed DUF679 membrane proteins. Nat. Plants *5*, 253–257. https://doi.org/10.1038/s41477-019-0382-3.

56. Takahashi, T., Mori, T., Ueda, K., Yamada, L., Nagahara, S., Higashiyama, T., Sawada, H., and Igawa, T. (2018). The male gamete membrane protein DMP9/DAU2 is required for double fertilization in flowering plants. Development *145*, dev170076. https://doi.org/10.1242/dev.170076.
57. Shilagardi, K., Li, S., Luo, F., Marikar, F., Duan, R., Jin, P., Kim, J.H., Murnen, K., and Chen, E.H. (2013). Actin-Propelled Invasive Membrane Protrusions Promote Fusogenic Protein Engagement During Cell-Cell Fusion. Science *340*, 359–363. https://doi.org/10.1126/science.1234781.
58. Faust, J.J., Balabiyev, A., Heddleston, J.M., Podolnikova, N.P., Baluch, D.P., Chew, T.-L., and Ugarova, T.P. (2019). An actin-based protrusion originating from a podosome-enriched region initiates macrophage fusion. MBoC *30*, 2254–2267. https://doi.org/10.1091/mbc.E19-01-0009.
59. Luo, Z., Shi, J., Pandey, P., Ruan, Z.-R., Sevdali, M., Bu, Y., Lu, Y., Du, S., and Chen, E.H. (2022). The cellular architecture and molecular determinants of the zebrafish fusogenic synapse. Dev. Cell *57*, 1582–1597.e6. https://doi.org/10.1016/j.devcel.2022.05.016.
60. Wilson, N.F., and Snell, W.J. (1998). Microvilli and cell-cell fusion during fertilization. Trends Cell Biol. *8*, 93–96. https://doi.org/10.1016/S0962-8924(98)01234-3.
61. Chen, E.H. (2011). Invasive Podosomes and Myoblast Fusion. In Current Topics in Membranes (Elsevier), pp. 235–258. https://doi.org/10.1016/B978-0-12-385891-7.00010-6.
62. Fox, S., Tran, A., Trinkle-Mulcahy, L., and Copeland, J.W. (2022). Cooperative assembly of filopodia by the formin FMNL2 and I-BAR domain protein IRTKS. J. Biol. Chem. *298*, 102512. https://doi.org/10.1016/j.jbc.2022.102512.
63. Zhao, H., Pykäläinen, A., and Lappalainen, P. (2011). I-BAR domain proteins: linking actin and plasma membrane dynamics. Curr. Opin. Cell Biol. *23*, 14–21. https://doi.org/10.1016/j.ceb.2010.10.005.
64. Ren, G., Vajjhala, P., Lee, J.S., Winsor, B., and Munn, A.L. (2006). The BAR Domain Proteins: Molding Membranes in Fission, Fusion, and Phagy. Microbiol. Mol. Biol. Rev. *70*, 37–120. https://doi.org/10.1128/MMBR.70.1.37-120.2006.
65. Brizzio, V., Gammie, A.E., and Rose, M.D. (1998). Rvs161p Interacts with Fus2p to Promote Cell Fusion in Saccharomyces cerevisiae. J. Cell Biol. *141*, 567–584. https://doi.org/10.1083/jcb.141.3.567.
66. Richard, J.-P., Leikina, E., Langen, R., Henne, W.M., Popova, M., Balla, T., McMahon, H.T., Kozlov, M.M., and Chernomordik, L.V. (2011). Intracellular curvature-generating proteins in cell-to-cell fusion. Biochem. J. *440*, 185–193. https://doi.org/10.1042/BJ20111243.
67. Yan, G., Ma, Y., Wang, Y., Zhang, J., Cheng, H., Tan, F., Wang, S., Zhang, D., Xiong, J., Yin, P., et al. (2024). A seven-sex species recognizes self and non-self mating-type via a novel protein complex. Preprint at Elife *13*, RP93770. https://doi.org/10.7554/eLife.93770.2.
68. Beaty, S.M., Park, A., Won, S.T., Hong, P., Lyons, M., Vigant, F., Freiberg, A.N., tenOever, B.R., Duprex, W.P., and Lee, B. (2017). Efficient and Robust *Paramyxoviridae* Reverse Genetics Systems. mSphere *2*. e00376-16. https://doi.org/10.1128/mSphere.00376-16.
69. Cassidy-Hanley, D.M. (2012). Tetrahymena in the Laboratory: Strain Resources, Methods for Culture, Maintenance, and Storage. In Methods in Cell Biology (Elsevier), pp. 237–276. https://doi.org/10.1016/B978-0-12-385967-9.00008-6.
70. Hayashi, A., and Mochizuki, K. (2015). Targeted Gene Disruption by Ectopic Induction of DNA Elimination in *Tetrahymena*. Genetics *201*, 55–64. https://doi.org/10.1534/genetics.115.178525.
71. Bruns, P.J., and Cassidy-Hanley, D. (2000). Biolistic transformation of macro- and micronuclei. Methods Cell Biol. *62*, 501–512.
72. Gao, S., Xiong, J., Zhang, C., Berquist, B.R., Yang, R., Zhao, M., Molascon, A.J., Kwiatkowski, S.Y., Yuan, D., Qin, Z., et al. (2013). Impaired replication elongation in *Tetrahymena* mutants deficient in histone H3 Lys 27 monomethylation. Genes Dev. *27*, 1662–1679. https://doi.org/10.1101/gad.218966.113.
73. Gibson, D.G., Young, L., Chuang, R.-Y., Venter, J.C., Hutchison, C.A., and Smith, H.O. (2009). Enzymatic assembly of DNA molecules up to several hundred kilobases. Nat. Methods *6*, 343–345. https://doi.org/10.1038/nmeth.1318.
74. Tian, M., and Loidl, J. (2018). A chromatin-associated protein required for inducing and limiting meiotic DNA double-strand break formation. Nucleic Acids Res. *46*, 11822–11834. https://doi.org/10.1093/nar/gky968.
75. Kataoka, K., Schoeberl, U.E., and Mochizuki, K. (2010). Modules for C-terminal epitope tagging of Tetrahymena genes. J. Microbiol. Methods *82*, 342–346. https://doi.org/10.1016/j.mimet.2010.07.009.
76. Mochizuki, K. (2008). High efficiency transformation of Tetrahymena using a codon-optimized neomycin resistance gene. Gene *425*, 79–83. https://doi.org/10.1016/j.gene.2008.08.007.
77. Lai, A.L., and Freed, J.H. (2014). HIV gp41 Fusion Peptide Increases Membrane Ordering in a Cholesterol-Dependent Fashion. Biophys. J. *106*, 172–181. https://doi.org/10.1016/j.bpj.2013.11.027.
78. Budil, D.E., Lee, S., Saxena, S., and Freed, J.H. (1996). Nonlinear-Least-Squares Analysis of Slow-Motion EPR Spectra in One and Two Dimensions Using a Modified Levenberg–Marquardt Algorithm. J. Magn. Reson., Ser. A *120*, 155–189. https://doi.org/10.1006/jmra.1996.0113.
79. Lai, A.L., and Freed, J.H. (2021). SARS-CoV-2 Fusion Peptide has a Greater Membrane Perturbating Effect than SARS-CoV with Highly Specific Dependence on Ca^2. J. Mol. Biol. *433*, 166946. https://doi.org/10.1016/j.jmb.2021.166946.
80. Lai, A.L., Millet, J.K., Daniel, S., Freed, J.H., and Whittaker, G.R. (2017). The SARS-CoV Fusion Peptide Forms an Extended Bipartite Fusion Platform that Perturbs Membrane Order in a Calcium-Dependent Manner. J. Mol. Biol. *429*, 3875–3892. https://doi.org/10.1016/j.jmb.2017.10.017.
81. Lai, A.L., and Freed, J.H. (2022). Negatively charged residues in the membrane ordering activity of SARS-CoV-1 and -2 fusion peptides. Biophys. J. *121*, 207–227. https://doi.org/10.1016/j.bpj.2021.12.024.
82. Liang, Z., and Freed, J.H. (1999). An Assessment of the Applicability of Multifrequency ESR to Study the Complex Dynamics of Biomolecules. J. Phys. Chem. B *103*, 6384–6396. https://doi.org/10.1021/jp9907746.
83. Ravoo, B.J., Weringa, W.D., and Engberts, J.B. (1999). Membrane Fusion in Vesicles of Oligomerizable Lipids. Biophys. J. *76*, 374–386. https://doi.org/10.1016/S0006-3495(99)77204-8.
84. Lai, A.L., Moorthy, A.E., Li, Y., and Tamm, L.K. (2012). Fusion Activity of HIV gp41 Fusion Domain Is Related to Its Secondary Structure and Depth of Membrane Insertion in a Cholesterol-Dependent Fashion. J. Mol. Biol. *418*, 3–15. https://doi.org/10.1016/j.jmb.2012.02.010.

STAR★METHODS

KEY RESOURCES TABLE

REAGENT or RESOURCE	SOURCE	IDENTIFIER
Antibodies		
Anti-HA Antibody 1:100, clone 3F10	Fisher Scientific	Cat# 50-100-3325; RRID: AB_390918
Goat Anti-Rat IgG, H & L Chain Specific Fluorescein Conjugate 1:400	MilliporeSigma	Cat# 401414; RRID: AB_437800
Chemicals, peptides, and recombinant proteins		
IC Fixation Buffer	Thermo Fisher	Cat# 00-8222-49
10x Permeabilization Buffer	Thermo Fisher	Cat# 00-8333-56
eBioscience Carboxyfluorescein diacetate succinimidyl ester	Thermo Fisher	Cat# 65-0850-84
CellTrace™ Far Red	Thermo Fisher	Cat# C34564
Lipofectamine 2000 Transfection Reagent™	Invitrogen	Cat# 11668-019
Hoechst 33342	Thermo Fisher	Cat# 62249
Lysozyme	MilliporeSigma	Cat# 10837059001
Halt™ Protease Inhibitor Cocktail	Thermo Fisher	Cat# 78429
Benzonase Nuclease	MilliporeSigma	Cat# E1014
Thrombin	MilliporeSigma	Cat# 10602400001
Bradford Dye Reagent	Thermo Fisher	Cat# J61522.AP
POPC Lipid	Avanti Polar Lipids	Cat# 850457
POPG Lipid	Avanti Polar Lipids	Cat# 840457
5PC Lipid	Avanti Polar Lipids	Cat# 878123
DPPTC Lipid	Avanti Polar Lipids	Cat# 850355
Octadecyl Rhodamine B chloride (R18)	Thermo Fisher	Cat# O246
Experimental models: Cell lines		
BSR-T7 cells[68]	Laboratory of Ben Benhur Lee (Icahn School of Medicine at Mount Sinai)	N/A
Rosetta (DE3) Competent Cells	MilliporeSigma	Cat# 70954-3
Experimental models: Organisms/strains		
B2086.2	Tetrahymena Stock Center	TSC_SD00709
CU427.4	Tetrahymena Stock Center	TSC_SD00715
CU428.2	Tetrahymena Stock Center	TSC_SD00178
SB1969	Tetrahymena Stock Center	TSC_SD00701
GFU1 KO MAC cl. 9	Tetrahymena Stock Center	TSC_SD03390
GFU1 KO MAC cl. 19	Tetrahymena Stock Center	TSC_SD03391
GFU1 KO MAC cl. 21	Tetrahymena Stock Center	TSC_SD03392
GFU2 KO MAC cl. B3	Tetrahymena Stock Center	TSC_SD03393
GFU2 KO MAC cl. C1	Tetrahymena Stock Center	TSC_SD03394
GFU2 KO MAC cl. C9	Tetrahymena Stock Center	TSC_SD03395
HAP2 KO MAC B2086 cl. B2	Tetrahymena Stock Center	TSC_SD03396
HAP2 KO MAC CU428 cl. B3	Tetrahymena Stock Center	TSC_SD03398
GFU1:HA MAC CU428 cl. 13	Tetrahymena Stock Center	TSC_SD03402
GFU1:HA MAC B2086 cl. 21	Tetrahymena Stock Center	TSC_SD03404
GFU1:mCherry MAC CU428 cl. 1	Tetrahymena Stock Center	TSC_SD03406

(*Continued on next page*)

Continued

REAGENT or RESOURCE	SOURCE	IDENTIFIER
GFU1:mCherry MAC B2086 cl. 36	Tetrahymena Stock Center	TSC_SD03408
GFU1:mCherry HAP2:GFP MAC CU522 cl.2	Tetrahymena Stock Center	TSC_SD03414
HAP2($R^{164}A$) MAC CU427 cl. 18	Tetrahymena Stock Center	TSC_SD03410
HAP2($R^{164}A$) MAC CU428 cl. 1	Tetrahymena Stock Center	TSC_SD03412
HAP2:GFP MAC CU522	Tetrahymena Stock Center	TSC_SD03418
Oligonucleotides		
See Table S1 for PCR Primers		
Recombinant DNA		
pCR™Blunt-TOPO®	Thermo Fisher	Cat# 451245
pmCherry-neo4	Tetrahymena Stock Center	PID00045
pHA-neo4	Tetrahymena Stock Center	PID00043
pMcoDel	Laboratory of Kazufumi Mochizuki	https://www.igh.cnrs.fr/en/research/departments/genetics-development/epigenetic-chromatin-regulation
pMiniT 2.0	New England Biolabs	Cat# E1202S
pET32a(+)	MilliporeSigma	Cat# 69015-3
Software and algorithms		
FlowJo	FlowJo LLC	https://www.flowjo.com/
GraphPad Prism 10	GraphPad Software	https://www.graphpad.com/
Alphafold Version 2.3.1	N/A	https://alphafold.ebi.ac.uk/
RaptorX	N/A	http://raptorx6.uchicago.edu/
Other		
Q5® Site-Directed Mutagenesis Kit	New England Biolabs	Cat# E0554S
6-well platesx	VWR	Cat# 734-2777
DMEM medium	Corning	Cat# 10-013-CV

RESOURCE AVAILABILITY

Lead contact

Further information and requests for resources and reagents should be directed to and will be fulfilled by the lead contact, Theodore Clark (tgc3@cornell.edu).

Materials availability

Tetrahymena strains generated in this study have been deposited to the Tetrahymena Stock Center at Washington University in St. Louis.

Data and code availability

- All data reported in this paper will be shared by the lead contact upon request.
- This paper does not report original code.
- Any additional information required to reanalyze the data reported in this paper is available from the lead contact upon request.

EXPERIMENTAL MODEL AND STUDY PARTICIPANT DETAILS

Growth of Tetrahymena thermophila strains

Tetrahymena strains of different mating type (MT) were grown separately to mid-log phase at 30°C with continuous shaking (100 rpm) in either NEFF medium (0.25% proteose peptone, 0.25% yeast extract, 0.5% glucose, 33.3 μM $FeCl_3$)[69] or SPP medium (2% proteose peptone, 0.1% yeast extract, 0.2% glucose, 33mM $FeCl_3$)[69] as indicated in the text.

METHOD DETAILS

Mating of Tetrahymena strains

To prepare mating cultures, cells were centrifuged at 400 x g for 2 min, washed in 10mM Tris buffer (pH 7.5), and then starved in the same buffer for 18–48 h at 30°C. Following starvation, cells of different mating type (MT) were counted, brought to final concentrations of 2.5 x 10^5 cells per mL and combined at a ratio of 1:1 in 10 cm diameter plastic petri dishes. Mating cultures were then maintained without shaking at 30°C before being analyzed. For all wild type x wild type matings, strains CU428.2 (MT = VII) and CU427.4 (MT = VI) were used.

Construction of *GFU1* and *GFU2* deletion strains

Different strategies were used to generate macronuclear gene disruptions of *GFU1* and *GFU2*. For *GFU1*, the "co-deletion" method was used, which relies on the inherent genome editing properties of *T. thermophila* during macronuclear development.[70] Briefly, a 1562-bp target sequence covering roughly two-thirds of the coding region between primers #1 and #2 (Table S1) in the predicted *GFU1* gene (Tetrahymena Genome Database: TTHERM_000161578) was cloned into a unique NotI site in the plasmid vector, pMcoDel.[70] The resulting construct contained the sequence targeted for deletion flanked by internally eliminated sequence motifs in a vector harboring the entire ribosomal DNA locus including a 17S rRNA allele which confers paromomycin resistance on transformed cells. Following vector construction, plasmid DNA was introduced into mating pairs of *T. thermophila* strains B2086.2 and CU428.2 at 7 h post-mixing using biolistic bombardment as described by Bruns and Cassidy-Hanley.[71] Cells were maintained overnight in 10 mM Tris (pH7.5), grown for 3 h in SPP medium, and drug-resistant positive transformants were selected by continuous growth in SPP containing 100 μg/mL paromomycin. A total of seven independent clones were identified, all of which showed the minimal 1562-bp deletion in the endogenous *GFU1* macronuclear DNA locus as determined by PCR using flanking primers. Complete elimination of the target sequence in all 45 macronuclear chromosomes was confirmed by quantitative PCR (qPCR) using primers #3 and #4 (Table S1) within the deleted region. Three clones designated GFU1 KO MAC cl. 9 (MT = II), GFU1 KO MAC cl. 19 (MT = V), and GFU1 KO MAC cl. 21 (MT = IV) were used in these studies.

For disruption of *GFU2*, we used homologous recombination to replace the entire open reading frame of the gene with a cadmium-inducible cycloheximide (CHX) resistance cassette described by Gao et al.[72] In this case, regions containing >700-bp immediately upstream and downstream of the predicted *GFU2* coding sequence (Tetrahymena Genome Database: TTHERM_00569470) were amplified in separate PCR reactions using primers #5-#8 (Table S1) and linked on either side of the CHX cassette in pBlueScript SK(+) by Gibson assembly.[73] Plasmid DNA was then linearized and introduced into *T. thermophila* (B2086.2 X CU428.2) mating pairs by biolistic bombardment as above.[71] Positive transformants were selected by growth in SPP medium containing increasing concentrations (from 15 to 240 μg/mL) of cycloheximide and 4.5 μg/mL $CdCl_2$.[72,74] Complete replacement of the endogenous *GFU2* gene by the CHX cassette was confirmed by qPCR using primers #9 and #10 (Table S1). Clonal isolates designated GFU2 KO MAC cl. B3 (MT = II), GFU2 KO MAC cl. C1 (MT = VII), and GFU2 KO MAC cl. C9 (MT = VII) were used for all experiments.

Construction of mutant strains

Cell lines carrying the *T. thermophila HAP2/GCS1* $R^{164}A$ mutant allele were constructed as previously described.[3] Briefly, site-directed mutagenesis was carried out to alter the sequence of the wild type *HAP2/GCS1* cDNA using a Q5 Site-Directed Mutagenesis Kit. The mutant cDNA was then amplified using primers N7_R64A_F and N7_R164A_R (Table S1) and directionally cloned between BamHI and KpnI restriction sites in a previously constructed replacement vector containing the pHrpl29-B cycloheximide resistance cassette in a pCRBlunt-*TOPO* plasmid backbone. This placed the mutant allele between roughly 1,000-bp segments immediately upstream or downstream of the 5′- and 3′-flanking regions of the *T. thermophila* HAP2/GCS1 gene, along with an HA-tag at the C-terminus of the HAP2/GCS1 coding sequence. Vector DNA was then linearized and introduced into the *T. thermophila* Δ*hap2/gcs1* knockout strains Δ*HAP2-428* clone 5 (MT = VII) and Δ*HAP2-427* clone 6 (MT = VI) by biolistic bombardment.[71] Positive transformants were isolated by growth in NEFF medium containing increasing concentrations of cycloheximide up to 50 μg/mL and their genomic DNA amplified and sequenced to establish the presence of the mutant allele.[3] Mutant strains in two different mating type backgrounds designated, HAP2(R^{164}A) MAC CU427 cl. 18 and HAP2(R^{164}A) MAC CU428 cl. 1, were used in these studies.

Construction of mCherry- and HA-tagged GFU1 expressing strains was carried out using a modified PCR-based C-terminal epitope tagging approach described by Kataoka et al.[75] and plasmid vectors containing codon-optimized sequences for mCherry or HA-epitope tags (pmCherry-neo4 and pHA-neo4, respectively). In each case, the tags were immediately upstream of a *T. thermophila* BTU1 3′-termination sequence and *neo*4 resistance cassette[76] within a pBluescript plasmid backbone. Plasmid DNA was used to amplify the region between the 5′-ends of the coding sequences of the mCherry or HA-epitope tags and the 3′-end of the *neo*4 cassette in separate PCR reactions using primers BamHI-mCherry_Fw1 and HindIII-Neo4-RV2 (for mCherry) or BamHI-HA_FW1 and HindIII-Neo4-RV2 (for HA) (Table S1). *T. thermophila* genomic DNA was then used as a template to amplify a roughly 1,000-bp segment immediately upstream of the 3′-stop codon in the macronuclear *GFU1* gene in two separate PCR reactions using the same forward primer (5′FW) and either of two linker primers designated 5′RV_mCherry and 5′RV_HA, respectively (Table S1). Lastly, a third segment extending 863-bp downstream of the 3′-end of the *GFU1* coding sequence was generated using the forward primer, 3′FW, and reverse primer, 3′RV (Table S1) with *T. thermophila* genomic DNA as the template. The PCR products from each of the reactions were then stitched together by overlap PCR. After agarose gel electrophoresis, bands of the expected sizes of the full-length products were purified and amplified with the 5′RACE-Outer and 3′RACE-Outer primers (Table S1) to create the 5′-*GFU1-mCherry-BTU1-neo-GFU1*-3′ and 5′-*GFU1-HA-BTU1-neo-GFU1*-3′ insertion cassettes. Insertion cassettes were then

cloned into the plasmid vector pMiniT 2.0 and sequenced. Plasmid DNA was linearized by treatment with *Xho*1 and introduced into the endogenous *GFU1* locus of *T. thermophila* strains CU428.2 (MT VII) and B2086.2 (MT II) by homologous recombination following biolistic bombardment.[71] Positive transformant clones were selected by growth in NEFF medium containing increasing concentrations of paromomycin (up to 800 μg/mL). Strains designated GFU1:HA MAC CU428 cl. 13, GFU1:HA MAC B2086 cl. 21, GFU1:mCherry MAC CU428 cl. 1 and GFU1:mCherry MAC B2086 cl. 36, were used in the present studies.

For co-localization experiments, the 5′-*GFU1-mCherry-BTU1-neo-GFU1*-3′ insertion cassette was also used to replace the endogenous *GFU1* gene in a previously generated *T. thermophila* strain, HAP2:GFP MAC CU522,[24] containing an inducible C-terminal GFP-tagged version of HAP2/GCS1 at the β-tubulin1 locus as described above. The resulting strain designated GFU1:mCherry HAP2:GFP MAC CU522 cl.2 (MT = IV) was used in the present study.

Δ*hap2/gcs1* deletion strains

The strains designated, HAP2 KO MAC B2086 cl. B2 (MT = II) and HAP2 KO MAC CU428 cl. B3 (MT = VII),[3,24] were obtained from the Tetrahymena Stock Center at Washington University in St. Louis and used in all crosses involving Δ*hap2/gcs1* deletion strains.

Pair stability assays

For undisturbed cultures, cells of complementary mating type were grown separately in NEFF medium to mid-log phase, then washed and starved as indicated above. Between 0 and 3 h post-mixing, aliquots were collected every 30 min by gentle pipetting and combined with an equal volume of IC Fixation Buffer in 1.5mL plastic microcentrifuge tubes. After 3 h, cells were fixed every hour until mating was complete (18–24 h post-mixing). The percentage of cells that were paired at each time point was then determined by counting a representative sample from each aliquot under a dissecting microscope as described below for mechanically agitated cells.

Strength of cell-cell pairing was determined as previously described.[24] Briefly, complementary mating types were grown and starved as above, then combined at ratios of 1:1. At 2 and 4 h post-mixing, 3mL of mating culture was removed and placed into a 15 mL plastic conical tube. The tube was then lowered onto a shaking Vortex-Genie 2 laboratory mixer set to speed 4.5. Cells were then vortexed for cumulative periods of 0 s, 2 s, 5 s, and additional 5 s intervals up to 45 s. At each time point, 50 μL aliquots were gently removed and fixed in an equal volume of IC Fixation Buffer. The percentage of cells paired at each time point was calculated by counting a representative sample from each of the fixed aliquots under a dissecting microscope. A total of 100 subjects (single cells or pairs) were counted for each time point with the percentage of pairs calculated as the number of paired cells divided by the number of total cells x 100.

Flow cytometric fusion assays

Unless otherwise noted, the ability of mating pairs to form fusion pores was quantitated by flow cytometry as described by Pinello and coworkers.[3] Briefly, cells of complementary mating types were grown separately in NEFF medium to mid-log phase prior to starvation in Tris buffer (pH 7.5) at 30°C overnight. Starved cells were then centrifuged and resuspended in 0.1x phosphate buffered saline (PBS) to a final concentration of 7 x 10^6 cells/mL. Aliquots of concentrated cells (1 mL) were combined with 1 mL 0.1x PBS containing either 2 mL Carboxyfluorescein diacetate succinimidyl ester (CFSE) or 5 mL CellTrace Far Red (CTFR) and incubated 5 min (CFSE) or 15 min (CTFR) before quenching unincorporated dye in 10 mL of NEFF medium. Labeled cells were pelleted at 400 x g, then washed twice and resuspended in 10 mM Tris • HCl buffer (pH 7.5) at 30°C in the dark. The next day, cells were resuspended in fresh 10 mM Tris • HCl buffer (pH 7.5) and recounted. Aliquots of 5 x 10^5 cells of each mating type were then combined in a total of 5 mL of 10 mM Tris buffer in triplicate plates, and either collected immediately or allowed to mate at 30°C for 18–36 h (as indicated in the text) in a darkened incubator. Following mating, cells were harvested by centrifugation at 400 x g, resuspended in 1 mL of 10 mM Tris buffer and combined with 1 mL of IC Fixation Buffer followed by incubation in the dark for a minimum of 20 min. After fixation, cells were again harvested and resuspended in 500 μL of 1x PBS (0.3% bovine serum albumin (BSA)) prior to acquisition on a FACSCanto II flow cytometer (Becton Dickinson) using the FITC-A and APC-CY7-A lasers. A minimum of 30,000 events were recorded for each sample. Data were analyzed using FlowJo version 10.4 software with gates of single- (unfused) and double-labeled (fused) cell populations being drawn as previously described.[3] Compiled data from all experiments for a given cross were assembled as bar charts using GraphPad Prism Software.

Fusion assays in mammalian cell culture

Full-length, codon-optimized cDNA sequences encoding *A. thaliana* HAP2/GCS1 and *T. thermophila* GFU1 and GFU2 were introduced into a pCAGGS plasmid expression vector (TWIST Bioscience) downstream of a cytomegalovirus early enhancer and chicken β-actin promoter and in-frame with the C-terminal tags Au1 (*A. thaliana* HAP2/GCS1); HA (GFU1); or FLAG (GFU2). For *T. thermophila* HAP2/GCS1, a full-length, codon-optimized version of the corresponding cDNA containing a C-terminal 3X-FLAG tag was cloned into the plasmid expression vector pcDNA3.1(+) as previously described by Pinello et al. For syncytia assays, BSR-T7 cells[68] (gift from Ben Benhur Lee, Icahn School of Medicine at Mount Sinai) were seeded onto 6-well plates and grown in 1x DMEM medium containing 10% bovine calf serum and 1% penicillin/streptomycin. When monolayers reached 80% confluence, cells were transfected with plasmid DNA using Lipofectamine 2000 Transfection Reagent according to the manufacturer's instructions. Constant concentrations of plasmid DNA across conditions were maintained by combining 1 μg HAP2/GCS1-encoding plasmid DNA with either empty vector (2 μg) or 1 μg each of vector DNA encoding *T. thermophila* GFU1 and GFU2. Expression of epitope-tagged proteins was verified 24 h post-transfection by western blotting and fluorescence microscopy

using labeled antibodies against specific tags in each case. Expression levels of the *Arabidopsis* and *Tetrahymena* HAP2/GCS1 proteins were roughly equivalent based on densitometry readings in western blots. To assay syncytia formation, cultures were fixed in 1x phosphate buffered saline (pH 7.4) containing 2% paraformaldehyde 30 h post-transfection and stained with Hoechst 33342 to label nuclei. Syncytia formation was quantified as previously described by measuring the total number of nuclei in syncytia per field in 4–7 random fields per experiment ($n = 3$) using an inverted microscope (ECHO Revolve) with phase optics at 10× magnification. A syncytium was considered any cell with ≥4 nuclei.

Fluorescence microscopy

For visualization of HA-tagged GFU1, mating *T. thermophila* cells were centrifuged at 400 x g, resuspended in 20 mM HEPES buffer (pH 7.5), and fixed with IC Fixation Buffer as described above for flow cytometry. Cells were then resuspended and washed three times in 1 mL of 1x Permeabilization Buffer in a 1.5 mL plastic microcentrifuge tube before being resuspended in blocking solution (1x Permeabilization buffer containing 5% Goat Serum and 1% BSA). The same blocking solution was used for all subsequent washes and antibody incubations. After blocking for a minimum of 30 min at room temperature, cells were again washed and then incubated at 4°C overnight in blocking solution containing a 1:100 dilution (100 μg/mL) of primary antibody (Anti-HA). Following incubation, cells were washed 3x in blocking solution before being incubated in the dark at RT with a 1:400 dilution (10 μg/mL) of fluorescein conjugated secondary goat Anti-Rat IgG (H + L). Following incubation, cells were washed 3x and resuspended in a small volume of blocking solution for imaging on a Leica SP5 confocal microscope.

For co-localization studies, a strain carrying an mCherry-tagged version of *GFU1* at the endogenous locus and an inducible GFP-tagged version of HAP2/GCS1 at the β-tubulin locus (see above) was induced with 0.1 μg/mL $CdCl_2$, 2 h prior to mating with wild type strain CU428.2 at a ratio of 1:1. At varying times thereafter, mating pairs were examined with an Olympus BX-50 fluorescence microscope equipped with a Fluoview scanning laser confocal imaging system and images were captured with a DP-72 digital camera.

Isolation of recombinant GFU1

The full-length GFU1 cDNA expressed in baby hamster kidney cells was subcloned into a pET32a(+) vector using the restriction enzymes KpnI and XhoI. The plasmid was then introduced into the Rosetta (DE3) *E. coli* strain designed for enhanced expression of eukaryotic proteins. Bacteria were grown to O.D. = 1.0 and *GFU1* expression was induced by addition of IPTG to the culture medium to a final concentration of 0.4 mM. Cells were maintained at 30°C overnight and harvested by centrifugation at 4000 × g for 30 min at 4° C.

Recombinant GFU1 was purified by affinity chromatography on Ni^{2+}-TED resin (PrepEase His-Tagged Protein Purification Maxi Kit, USB Corp, Cleveland, OH). Cell pellets were resuspended 1× LEW buffer (50mM NaH_2PO_4, 300mM NaCl, pH.8) at a ratio of 10 mL buffer for every 1 L of cells harvested before addition of 1 mg/mL lysozyme, 100 μL Halt Protease Inhibitor Cocktail, and 2μL Benzonase nuclease. After 30 min on ice, bacteria were sonicated for 5 min using a 30 s on/30 s off cycle in an ice water bath using an SXSONIC Ultrasonic Processor FS-450N sonicator (Hengyi, China) set to 40% power. The cell lysate was then centrifuged at 12,000 x g for 30 min at 4°C in a Beckman Coulter Allegra X-14R high-speed centrifuge. Supernatants were collected and applied to a pre-equilibrated Ni-TED column following the manufacturer's protocol. The column was washed twice with 1 x LEW buffer and proteins were stripped from the column in 3 fractions of 4 mL each with 1 x LEW buffer containing 250 mM Imidazole, pH.8). Eluted fractions were dialyzed overnight at 4°C against 150 mM NaCl, 20 mM HEPES, and 5mM MES buffer, pH7 in the presence of 100μL thrombin to remove the His tag. The dialyzed product was then applied to a pre-packed size exclusion column (Superdex 75 Increase) (Cytiva, Marlborough, MA) in fresh dialysis buffer and the fraction corresponding to GFU1 concentrated by ultrafiltration (Amicon Ultra Centrifugal filters; MWCO = 10kDa). Protein concentrations were determined using a Bradford Dye Reagent and purified GFU1 stored at 4°C for 1–3 days before use.

Lipid ESR assays

All lipids including POPC (1-palmitoyl-2-oleoyl-*glycero*-3-phosphocholine); POPG (1-palmitoyl-2-oleoyl-*sn*-glycero-3-phospho-(1′-rac-glycerol); the acyl chain spin label 5PC; and, the head group spin label, dipalmitoylphosphatidyl-tempo-choline (DPPTC), were purchased from Avanti Polar Lipids (Alabaster, AL). Structures of the spin labeled lipids used in the experiments are shown in Figures 4A and 4B. Cholesterol was purchased from Sigma-Aldrich. Composition of the fusion peptides from influenza HA and *T. thermophila* HAP2 were previously described.[3,54] The negative control peptide consisted of a random sequence derived from the wild type HAP2 fusion peptide. All peptides had a "GGGKKKK" solubility tag added to their C′ termini.[77]

POPC, POPG, cholesterol, and 0.5% (mol:mol) spin-labeled lipids dissolved in chloroform were mixed at a 5:2:3 mol:mol ratio of POPC:POPG:Chol and dried under a N_2 stream. The mixture was evacuated under vacuum overnight to remove any trace of chloroform. To prepare multilamellar vesicles (MLVs), the lipids were resuspended and hydrated prior to use in 1 mL of 150 mM NaCl, 10 mM MES, 5 mM HEPES (pH5) buffer at RT for at least 2 h. For the large unilamellar vesicles (LUVs) used in lipid mixing assay (below), lipids were prepared in the same buffer as for MLVs and then frozen and thawed 5 times prior to dispersion through a 100 nm pore size membrane using an Avanti extruder.

To prepare samples for ESR, stock solutions of each fusion peptide (1 mg/mL) or GFU1 (0.3 mM) were added to the lipid POPC:POPG:Chol = 5:2:3 MLV dispersion (above) at the experimentally indicated mol:mol protein(peptide):lipid ratios. After 20 min of incubation, the dispersion was centrifuged at 13,000 rpm for 10 min and the pellet was transferred to a quartz capillary tube for ESR measurement. ESR spectra were collected on an ELEXSYS ESR spectrometer (Bruker Instruments) at X-band (9.5 GHz) at 25°C using a N_2 Temperature Controller (Bruker Instruments). The ESR spectra from labeled lipids were analyzed using the NLLS fitting program based on the stochastic

Liouville equation[78] using the MOMD (Microscopic Order Macroscopic Disorder) model as in previous studies.[79–81] The fitting strategy is the same as previously reported.[49] S_0 is defined as follows: S_0=<1/2(3cos2θ-1)>, where θ is the polar angle for the orientation of the rotating axes of the nitroxide bonded to the lipid relative to the director of the bilayer, i.e., the preferential orientation of lipid molecules.[82] The angular brackets imply ensemble averaging. S_0 indicates how well the chain segment to which the nitroxide is attached is aligned along the normal to the lipid bilayer. The change in order parameter ΔS_0 is calculated as the S_0(membrane with protein) – S_0 (membrane only). All experiments were repeated three times.

Fluorescence dequenching assay

The protocol for fluorescence dequenching to monitor vesicle fusion was adopted from a previous study.[83] Fluorescently labeled LUVs (2.5 μM, final concentration) containing 2% Octadecyl Rhodamine B chloride and unlabeled LUV (22.5 μM, final concentration) were mixed in 1 mL 150 mM NaCl, 10 mM MES, 5 mM HEPES (pH 5.0) buffer. Proteins were then added from concentrated stock solutions to give a 1 μM final concentration of each peptide. Triton X-100 was added to achieve a 1% final concentration after fusion reactions were complete. The fluorescence spectra were collected on a Varian Cary Eclipse Fluorescence Spectrometer (Agilent Technologies). Fluorescence intensities of the samples before addition of fusion peptides and after the addition of Triton X-100 were used to set the baseline (0%) and 100% fusion levels, respectively. The fluorescence yields of the experimental samples were normalized to these levels to determine % lipid mixing.[84] Fluorescence intensity variations resulting from volume changes were corrected in each case.

Ultrastructural studies

For wild type and Δ*gfu1* deletion strains, mating cultures were prepared in 10 cm diameter plastic petri dishes as described above and at either 2 h or 4 h post-mixing, 10 mL aliquots of mating cells were gently harvested by centrifugation at 300 x g for 2min. Supernatants were quickly aspirated leaving a loose pellet in a total volume of 250–300 mL. Cells were then gently resuspended by pipetting, and 5 mL of fixation solution containing 2.5% glutaraldehyde in sodium cacodylate, pH 7.4 (Electron Microscopy Sciences, Fischer Scientific; Catalog #50-259-41) was added. Percent pairing in all cultures was ≥75% by microscopic evaluation. Cells were stored in fixation solution at 4° C until further use (4–11 days). For embedding and sectioning, samples were brought to 20°C, washed 1X in double-distilled H_2O, then 2x in 0.15M sodium cacodylate buffer pH 7.2 for 10 min per wash prior to post-fixation in 2% osmium tetroxide in 0.15M sodium cacodylate buffer pH 7.2 for 1 h. Samples were then washed 3x in H_2O (10 min/wash) and the cell pellets embedded in 2% agar for the remainder of the procedure to maintain the integrity of cell pairs. Samples were then fixed *en bloc* in 2% aqueous uranyl acetate for 60 min before dehydration in an ascending series of ethanol solutions of 35%, 50%, 75%, 95%, 100% ethanol for 10 min each. Ethanol was then replaced with propylene oxide in three consecutive 10 min incubations. Dehydrated blocs were infiltrated with Spurr's medium through a series of 1 h incubations in a 1:1 mixture of propylene oxide:Spurr's resin mixture, then a 1:2 mixture, then a 1:3 mixture, and finally 2 × 1 h incubations in fresh 100% Spurr's resin. Samples were cured at 70°C for at least 8 h. Samples were sectioned and placed on uncoated Formvar grids. Sections (~70 nm) were post-stained with lead citrate prior to imaging at 80kV on a Hitachi HT7700 transmission electron microscope.

Protein structure modeling

The 3D structure predictions of GFU1 and GFU2 were done with a local installation Alphafold[46] version 2.3.1 at the Institut Pasteur, using the latest release of the protein databank available in March 2023. Only predictions with highest scores are displayed in the Figures. Additionally, we used the RaptorX[42] algorithm to model the structure of GFU1. Details of P-value, Score, uGDT/GDT, and uSeqID/SeqID in the table in Figure 3E are provided at http://raptorx6.uchicago.edu/documentation/.

QUANTIFICATION AND STATISTICAL ANALYSIS

Data reported are expressed as the mean ± SD and statistical significance was determined with GraphPad Prism using the number of replicates and appropriate statistical test as reported in figure legends. A value of $p < 0.05$ was considered statistically significant.